

1 ***Arabidopsis thaliana* early foliar proteome response to root exposure**
2 **to the rhizobacterium *Pseudomonas simiae* WCS417**

3

4 Francesca Marzorati¹, Rossana Rossi², Letizia Bernardo², Pierluigi Mauri², Dario Di Silvestre²,
5 Emmanuelle Lauber³, Laurent D. Noël³, Irene Murgia^{1*}, Piero Morandini¹.

6

7 ¹ Department of Environmental Science and Policy, University of Milan, Milan, Italy

8 ² Proteomic and Metabolomic Laboratory, Institute for Biomedical Technologies- National

9 Research Council (ITB-CNR), Segrate, Italy

10 ³ Laboratoire des interactions plantes-microbes-environnement CNRS-INRAE, University of
11 Toulouse, Castanet-Tolosan, France

12

13

14 *Correspondence: irene.murgia@unimi.it

15

16

17

18

19

20

21

22

23

24

25 **Abstract**

26 *Pseudomonas simiae* WCS417 is a plant growth-promoting rhizobacterium that improves plant health
27 and development. In this study, we investigate the early leaf responses of *Arabidopsis thaliana* to
28 WCS417 exposure and the possible involvement of formate dehydrogenase (FDH) in such responses.
29 *In vitro*-grown *A. thaliana* seedlings expressing a FDH::GUS reporter show a significant increase in
30 FDH promoter activity in their roots and shoots after 7 days of indirect exposure (without contact) to
31 WCS417. After root exposure to WCS417, the leaves of FDH::GUS plants grown in the soil also
32 show an increased FDH promoter activity in hydathodes. To elucidate early foliar responses to
33 WCS417, as well as FDH involvement, the roots of *A. thaliana* wt Col and *atfdh1-5* knock-out mutant
34 plants grown in soil were exposed to WCS417 and proteins from rosette leaves were subjected to
35 proteomic analysis. The results reveal that chloroplasts, in particular several components of the
36 photosystems PSI and PSII, as well as members of the Glutathione S-transferase GST family, are
37 among the early targets of the metabolic changes induced by WCS417. Taken together, the alterations
38 in the foliar proteome, as observed in the *atfdh1-5* mutant, especially after exposure to WCS417 and
39 involving stress-responsive genes, suggest that FDH is a node in the early events triggered by the
40 interactions between *A. thaliana* and the rhizobacterium WCS417.

41

42 **Keywords**

43 *Arabidopsis thaliana*, formate dehydrogenase FDH, glutathione -S-transferases GST, hydathodes,
44 proteome, *Pseudomonas simiae* WCS417, rhizobacterium.

45 **Introduction**

46 Plant growth-promoting rhizobacteria (PGPR) can enhance plant development and defense through
47 their antagonist actions against soil plant pathogens (Wang et al. 2021). *Pseudomonas* is a competitive
48 bacterial genus in the rhizosphere (Simons et al. 1996; de Weert et al. 2002). In particular, its species
49 *simiae* WCS417 (previously known as *Pseudomonas fluorescens* WCS417) (Berendsen et al. 2015)
50 is one of the most characterized PGPR for the activation of the Induced Systemic Response ISR
51 (Pieterse et al. 2020). The molecular basis of ISR has been thoroughly investigated in *Arabidopsis*
52 *thaliana* roots colonized by WCS417 (Stringlis et al. 2018a; Zamioudis et al. 2014); ISR response
53 partially overlaps with the iron (Fe) deficiency response in *A. thaliana* (Romera et al. 2019). Volatile
54 organic compounds (VOCs) and Fe-chelating siderophores produced by PGPR trigger plant Fe uptake
55 pathways (Trapet et al. 2021; Verbon et al. 2019). Plants suffering from Fe deficiency may recruit
56 more siderophore-producing bacteria than plants growing under normal nutritional conditions (Jin et
57 al. 2006, 2010), and VOCs generated by ISR-inducing bacteria may relieve nutritional stress induced
58 by low Fe levels (Zamioudis et al. 2015; Zhang et al. 2009). In addition, WCS417 promotes the
59 expression of plant genes activated by low Fe levels, such as MYB72 (Palmer et al. 2013; Zamioudis
60 et al. 2015).

61 A recent transcriptional analysis of roots and shoots of *A. thaliana* seedlings inoculated with WCS417
62 suggested that the beneficial effects of WCS417 on plant growth and development are achieved by
63 modulation of sugar transport, the sucrose transporters SWEET11 and SWEET12 are indeed involved
64 in the growth-promoting effects of WCS417 (Desrut et al. 2020).

65 Formate dehydrogenase enzymes (FDHs) are found in bacteria, fungi, and plants (Alekseeva et al.
66 2011); plant FDHs, localized in mitochondria (Choi et al. 2014; Herman et al. 2002) and chloroplasts
67 (Lee et al. 2022; Olson et al. 2000), catalyze the oxidation of formate (HCOO^-) to CO_2 with the
68 reduction of NAD^+ to NADH. FDHs are referred to as 'stress enzymes' because their expression is
69 upregulated in response to several abiotic stresses (Ambard-Bretteville et al. 2003; Andreadeli et al.
70 2009; David et al. 2010; Hourton-Cabassa et al. 1998; Kurt-Gür et al. 2018; Li et al. 2002; Lou et al.

71 2016; Murgia et al. 2020; Suzuki et al. 1998). Only a few studies have shown FDH involvement in
72 the response to bacterial infections (Choi et al. 2014; David et al. 2010; Lee et al. 2022; Marzorati et
73 al. 2021).

74 WCS417 represents a model for studying the interactions between plants and beneficial rhizobacteria
75 (Pieterse et al. 2020 and references therein). However, little is still known about the molecular
76 changes occurring at the foliar level, upon plant root exposure to WCS417, as most studies have
77 focused on the rhizobacterial effects on roots several days after exposure (Trapet et al. 2016; Verbon
78 et al. 2019; Wintermans et al. 2016; Zamioudis et al. 2013).

79 Given these premises, the goal of the present study is to explore the early foliar responses of *A.*
80 *thaliana* to WCS417, and the involvement of FDH in such responses; such an approach could shed
81 light not only on the plant defense strategies, but also on the growth-promoting effects of WCS417
82 on the aerial parts of plants.

83 For that, the activity of the FDH promoter was first investigated in response to WCS417. The
84 colonization of roots, by WCS417, in seedlings of wt and of an FDH knock-out mutant (*atfdh1-5*)
85 was also investigated. Proteomic analysis of leaves of both wt Col and *atfdh1-5* mutant, after
86 their roots exposure to the rhizobacterium, was then performed.

87 Such analysis shows that FDH levels increase after exposure to WCS417, thus confirming FDH
88 involvement in the early *A. thaliana* foliar responses to WCS417, not only in terms of FDH promoter
89 activity but also at the protein level. Moreover, proteomic analysis reveals that chloroplasts, in
90 particular some proteins of photosystems I and II, as well as various members of the Glutathione S-
91 transferases family, are early targets of the adaptive plant response to WCS417. Finally, the
92 comparison of wt Col and *atfdh1-5* leaf proteomes reveals a different regulation of some stress-
93 responsive genes between the two lines, particularly after WCS417-treatment, suggesting FDH
94 involvement in the early stages of the interactions between *A. thaliana* and the rhizobacterium
95 WCS417.

96

97 **Results**

98 *Pseudomonas simiae* WCS417 rapidly induces FDH promoter activity in hydathodes

99 FDH is expressed in the leaves of *A. thaliana*, especially in hydathodes (Murgia et al. 2020), where
100 it is involved in early defense responses against the pathogen *Xanthomonas campestris* pv. *campestris*
101 (*Xcc*): it recently emerged that *Xcc* infection reduces FDH expression in wt leaves and that the spread
102 of an *Xcc* strain expressing GUS is more pronounced in the *atfdh1-5* mutant (Marzorati et al. 2021).
103 Consistently with these results, the *atfdh1-5* mutant is more susceptible to the virulent *Xcc* strain
104 8004 Δ *xopAC*: the disease index (DI), scored 7 days after wound-inoculation with bacterial
105 suspensions *Xcc* strain 8004 Δ *xopAC*, is significantly higher in *atfdh1-5* than in wt plants (**Figure S1**).
106 The effect of the plant growth-promoting rhizobacteria WCS417 on FDH expression was hence
107 explored. To this end, 7 days old *A. thaliana* *Vu* FDH::GUS seedlings (Murgia et al. 2020) were co-
108 cultivated *in vitro* with WCS417, for up to 7 more days, avoiding however any direct contact between
109 the seedlings and the rhizobacterium (or the mock solution) (**Figure 1A**). After 2 or 7 days of co-
110 cultivation, GUS staining of the seedlings revealed an increased FDH promoter activity in WCS417-
111 treated ones, in both roots and shoots; the latter were stained in the vascular tissue and hydathodes of
112 the rosette leaves (**Figure 1B, D**) compared to mock-treated seedlings (**Figure 1C, D**). Hence,
113 beneficial rhizobacteria can induce FDH expression in *A. thaliana* grown *in vitro*. Interestingly, such
114 an effect is opposite to the described effect of the pathogen *Xcc* on FDH expression (Marzorati et al.
115 2021).

116 To better evaluate how rapidly WCS417 may affect FDH expression in plants grown in soil, the roots
117 of 4 weeks old *A. thaliana* *Vu* FDH::GUS plants grown in soil were exposed to WCS417 by direct
118 inoculation of the bacterium into the soil, and their rosette leaves were stained for GUS activity. After
119 2 days, a higher number of stained hydathodes was observed in the rosette leaves of WCS417-treated
120 plants than in those of mock-treated plants (**Figure 2A**). To assess whether the treatment with
121 WCS417 could have altered leaf physiology, the common parameters for photochemical efficiency,

122 *i.e.*, F_0 (initial), F_m (maximum), F_v (variable) fluorescence, and the maximum photochemical
123 efficiency (F_v/F_m) were evaluated; these parameters are statistically similar in mock and *P. simiae*-
124 treated samples (**Figure S2A, B**). The induction of FDH promoter activity *in vitro*, without contact
125 between rhizobacteria and roots, suggests that WCS417 could affect FDH expression through the
126 emission of volatile compounds. To investigate this possibility *in vivo*, plants were organized in rows
127 in Aratrays to keep those positioned at the edges (named ‘close to WCS417’) fully isolated from those
128 positioned at the tray center; indeed, an entire row of empty baskets was positioned between the two
129 groups (**Figure S3A**). The roots of the plants positioned in the central rows were exposed to WCS417
130 by direct inoculation of WCS417 into the soil pots; the whole tray was then covered with a lid without
131 holes, to avoid dispersal of volatile compounds, and plants were not watered during the following 4
132 days to avoid any cross-contamination with *P. simiae* (**Figure S3B**). The same plant arrangement and
133 treatment were also performed for mock-treated plants and the ‘close to mock’ ones. Sampling of the
134 leaves from all plants (WCS417-treated, mock-treated, close to WCS417-treated, close to mock) was
135 then performed after 4 days, *i.e.*, after 2 more days with respect to what was described in **Figure 2A**,
136 to better assess the possible effects of volatile compounds. After 4 days, the induction of FDH
137 promoter activity could be observed with a higher number of GUS-stained hydathodes in WCS417-
138 treated plants than in mock-treated plants (**Figure 2B**); the slightly higher number of stained
139 hydathodes observed in the leaves of the plants positioned in the external lines (which did not receive
140 WCS417 themselves) is however not statistically different from what was observed in their mock
141 counterpart (**Figure 2B**).

142

143 *Colonization of atfdh1-5 roots by WCS417 is more pronounced than of wt roots*

144 The well-established morphological root responses to WCS417, *i.e.*, inhibition of root elongation,
145 promotion of lateral root formation, and root hair development (Zamioudis et al. 2013) were observed
146 in 7 days old wt seedlings, co-cultivated *in vitro* with WCS417 for 7 more days, without any initial
147 direct contact between the seedlings and the rhizobacterium (**Figure S4, S5-S6**). The *atfdh1-5* mutant,

148 in the same experimental condition, also showed enhanced root hair development with respect to its
149 mock counterpart (**Figure S4, S7-S8**), whereas the inhibition of root elongation and the promotion of
150 lateral root formation were less obvious in such mutant (**Figure S4, S7-S8**); this is likely due to its
151 short roots phenotype, as previously described (Murgia et al. 2020). Nonetheless, roots of *atfdh1-5*
152 seedlings grown on MS medium are colonized by WCS417 even better than wt roots (**Figure 3**).

153

154 *The chloroplasts, Glutathione S-transferases, and stress-responsive proteins are early targets in the*
155 *metabolic changes induced by WCS417*

156 To investigate the effect of WCS417 on aerial parts of plants, seedlings of both wt Col and *atfdh1-5*
157 were grown in either control or alkaline soil (pH 7.6) (**Figure S9**); WCS417 was then inoculated into
158 the soil in the proximity of the roots, and chlorophyll content and fresh weight (FW) of single rosettes
159 were evaluated after 8 days. As expected, the FW of both lines in the control soil was higher than at
160 pH 7.6 (**Figure S10A**). The chlorophyll content, for each line, was similar in both growth conditions
161 (**Figure S10D**); this lack of difference is partly because very small plants, *i.e.*, those more affected
162 by growth in alkaline soil (**Figure S9**), impact chlorophyll values less than healthier plants.

163 Notably, WCS417 treatment reduced the differences of FW in wt plants grown in control soil,
164 suggesting that WCS417 has a genuinely positive effect on growth, at least in control soil (**Figure**
165 **S10B**); this WCS417 growth-promoting effect is not observed in the *atfdh1-5* mutant (**Figure S10C**)
166 nor on the chlorophyll content of both lines (**Figure S10E, F**). The observed early changes in FDH
167 expression suggest that WCS417 can also affect the metabolic and signaling pathways in *A. thaliana*.
168 To uncover early rearrangements of these pathways and, in particular, the specific role of FDH in
169 these WCS417-induced networks, the roots of 4 weeks old wt Col plants and *atfdh1-5* mutant were
170 exposed to WCS417; after 2 days, rosette leaves were sampled for proteomic analysis. WCS417
171 treatment slightly decreases the weight of the rosettes in the wt, but not in the *atfdh1-5*, which
172 increases in weight (**Figure S11**).

173 Proteomic analysis was then performed on total proteins extracted from leaves: LC-MS/MS analysis
174 from untreated (wt Col mock, *atfdh1-5* mock) or exposed to WCS417 (wt Col WCS417, *atfdh1-5*
175 WCS417) samples allowed the identification of a total of 2196 distinct proteins (**Table S1**). About
176 16% of the total proteins had an average Peptide Spectrum Match (PSM) higher than 1 (**Figure 4A**,
177 blue and red dots). Globally, for each condition and genotype, about one thousand proteins were
178 identified, half of which were shared in pairwise comparisons (**Figure 4B**): 918 and 912 proteins
179 were detected in mock-treated wt Col and *atfdh1-5* plants, respectively, whereas 998 and 1066
180 proteins were detected in wt and *atfdh1-5* plants exposed to WCS417, respectively. A label-free semi-
181 quantitative comparison among the characterized protein profiles (wt Col mock vs wt Col WCS417,
182 *atfdh1-5* mock vs *atfdh1-5* WCS417, wt Col mock vs *atfdh1-5* mock, and wt Col WCS417 vs *atfdh1-5*
183 WCS417) allowed the extraction of total 362 Differentially Expressed Proteins (DEPs) (**Table S2**).
184 Major differences emerge between wt Col mock and wt Col WCS417 (150 DEPs, $P \leq 0.05$; 63 DEPs,
185 $P \leq 0.01$) (**Figure 5A, Table S3**) and between *atfdh1-5* mock and *atfdh1-5* WCS417 (268 DEPs, $P \leq$
186 0.05 ; 161 DEPs, $P \leq 0.01$) (**Figure 5B, Table S4**).

187 The functional evaluation of the characterized proteomes reveals a major enrichment of metabolic
188 processes (amino acid, carbon, nitrogen metabolism, and protein synthesis) in both genotypes
189 exposed to WCS417 (**Table S5**), which is more pronounced in the *atfdh1-5* treated with WCS417. In
190 this scenario, the presence of WCS417 correlates with the enrichment of other interesting pathways,
191 including photosynthesis, stress response, immune response, and transcription/translation. Notably,
192 FDH increases in WCS417-treated samples of wt Col (**Tables S1, S2**), thus confirming the data on
193 FDH promoter activity at the protein level; as expected, FDH was absent in the foliar proteomes of
194 the *atfdh1-5* mutant (**Tables S1, S2**) regardless of treatment.

195 Among the identified WCS417-upregulated proteins, 10 are shared between wt Col and *atfdh1-5*
196 (**Table 1**); among the WCS417-downregulated proteins, 19 are shared between wt Col and *atfdh1-5*
197 (**Table 2**). Therefore, these 29 WCS417-regulated proteins shared between the wt and the mutant line

198 are early targets of the changes mediated by WCS417 treatment in an FDH-independent manner. The
199 group of upregulated proteins (**Table 1**) is composed of two glutathione transferases (GSTF7 and
200 GSTF8), two subunits of vacuolar-type H⁺-ATPase VHA-B1 and VHA-C, three proteins with
201 housekeeping functions (translation initiation factor 4A1 EIF4A1, ribosomal proteins RPS1, and
202 RPS18C), and three plastidial proteins, that are the ATP synthase subunit beta atpB, a ribose-5-
203 phosphate isomerase RPI3, and a lipid-associated protein PAP6, also known as fibrillin 4. GSTs of
204 the Phi type, formerly known as type I, are involved in the response to abiotic and biotic stresses
205 (Sylvestre-Gonon et al. 2019); the expression of GSTF7 and GSTF8 is modulated by salicylic acid
206 (SA) (Sappl et al. 2004). V-type H⁺-ATPase is formed by various subunits with complex regulation
207 and is involved in stress adaptation (Dietz et al. 2001; Li et al. 2022); VHA-B1 is involved in the
208 modeling of the actin cytoskeleton (Ma et al. 2012). Among the four *A. thaliana* RPI isoforms, RPI1
209 is involved in actin organization (Huang et al. 2020); however, to date, no physiological functions
210 have been assigned to RPI3. PAP6 is involved in the resistance to biotic and abiotic stresses (Singh
211 et al. 2010).

212 Among the WCS417-downregulated proteins (**Table 2**), several of them are localized in plastids and,
213 in particular, are part of the photosynthetic electron transport chain: PSAE1 and PSAE2 are subunits
214 IV A and B of photosystem I; PSBP1 is an oxygen-evolving enhancer protein required for
215 photosystem II organization (Yi et al. 2007); PBS27-1 is a repair protein involved in photosystem II
216 assembly (Cormann et al. 2016); PSBO2 is the oxygen-evolving enhancer protein 1-2, required for
217 the regulation of the D1 reaction center of photosystem II (Lundin et al. 2007); CP29 is a minor
218 monomeric component of the PSII light-harvesting complex that, when phosphorylated, contributes
219 to PSII state transition and disassembly (Chen et al. 2013). Among the WCS417-downregulated
220 proteins that are localized in the plastid, there are also the chaperonins CPN10-2 and CPN20, the
221 ribosome recycling factor RRF required for chloroplast biogenesis (Wang et al. 2010), the RNA-
222 binding protein RGGC characterized by the arginine-glycine-glycine (RGG) region, the thylakoid
223 soluble phosphoprotein F13I12.120, and one unknown protein encoded by the At2g21530 gene

224 **(Table 2)**. A few WCS417-downregulated proteins are localized in the nucleus, *i.e.*, the RNA-binding
 225 protein RGG1 involved in the response to salt and drought stresses (Ambrosone et al. 2015), the
 226 negative regulator of cold acclimation cold shock protein 2 CSP2 (Sasaki et al. 2013), the core
 227 component of the nucleosome Histone H2B.9 (At5g02570) and an essential embryogenesis protein
 228 MEE59 (Pagnussat et al. 2005). Last, three more proteins were also identified as WCS417-
 229 downregulated proteins: the stress-responsive ERD10, which belongs to the dehydrin family and is
 230 expressed in particular under different abiotic stresses (Sun et al. 2021), calmodulin 7 CAM7
 231 (Kushwaha et al. 2008), and a protein of unknown function encoded by the At5g24165 gene (**Table**
 232 **2**).

233 The comparison of mock-treated wt Col and *atfdh1-5* proteomes identified 17 DEPs ($P \leq 0.01$) (61
 234 DEPs, $P \leq 0.05$) (**Figure 5C, Table S6A**) whereas the comparison of WCS417-treated wt Col and
 235 *atfdh1-5* proteomes identified 30 DEPs ($P \leq 0.01$) (84 DEPs $P \leq 0.05$) (**Figure 5 D, Table S6B**).
 236 These results are consistent with the correlation scores of the spectral counts compared in pairs:
 237 comparisons of the mock-treated (wt Col mock and *atfdh1-5* mock) and the WCS417-treated
 238 genotypes (wt Col WCS417 and *atfdh1-5* WCS417) have higher correlation values ($r \sim 0,8$) than the
 239 other comparisons, which show lower correlation values (**Figure 5E**).

240 Notably, seven enzymes involved in ROS-detoxification are differentially expressed in wt Col and/or
 241 *atfdh1-5* under mock or WCS417 treatment (**Table 3**), *i.e.*, six Glutathione Transferases (GSTF2,
 242 GSTF7, GSTF8, GSTF9, GSTF1, GSTU19) and the ascorbate peroxidase 1 APX1, which scavenges
 243 cytosolic H_2O_2 (Hong et al. 2022); in particular, APX1 is the only ROS detoxification protein that is
 244 upregulated in *atfdh1-5* leaves under both conditions (mock and WCS417-treated) with respect to wt
 245 Col counterparts (**Figure 5C, D and Table S6 A, B**). Interestingly, leaves of wt Col and *atfdh1-5*
 246 stained with diaminobenzidine (DAB) to detect any changes in the levels of hydrogen peroxide
 247 (H_2O_2) after WCS417 exposure, appear less brown-colored than their mock counterparts, suggesting
 248 that the rhizobacterium reduces the level of ROS (**Figure S12**).

249 Various other proteins involved in resistance to oxidative stress were also upregulated in *atfdh1-5*;
250 the Pathogenesis-Related protein 5 PR5 (At1g75040), involved in the activation of the SA signaling
251 pathway (Ali et al. 2018), is upregulated in mock-treated *atfdh1-5* compared to its wt Col counterpart
252 (**Figure 5C, Table S6A**), whereas PER34, GLO2, and ACO3 are upregulated in WCS417-treated
253 *atfdh1-5* compared to their wt Col counterparts (**Figure 5D, Table S6B**). Vice versa, the lipoxygenase
254 LOX2 required for jasmonic acid (JA) biosynthesis in leaves (Yang et al. 2020) is downregulated in
255 WCS417-treated *atfdh1-5* leaves compared to the wt (**Figure 5D, Table S6B**).

256

257

258 **Discussion**

259 Formate dehydrogenase (FDH) is a nutritional hub for iron (Fe) and molybdenum (Vigani et al. 2017;
260 Di Silvestre et al. 2021) and it also takes part in the plant response against the pathogen *Xanthomonas*
261 *campestris* pv *campestris*, especially in hydathodes (Marzorati et al. 2021). This latter evidence
262 prompted us to investigate the possible involvement of FDH in the plant response to the beneficial
263 growth-promoting rhizobacterium *Pseudomonas simiae* WCS417. In the present work, we
264 demonstrate that the FDH promoter is activated in both roots and shoots of seedlings exposed to
265 WCS417 and that this activation is quite rapid, as it could be detected in the hydathodes of the rosette
266 leaves just 2 days after root exposure to WCS417. We also demonstrate that, at least when seedlings
267 are grown *in vitro*, the observed effects may be mediated by rhizobacterium-produced volatile
268 compounds, consistent with previous studies (Wintermans et al. 2016; Zamioudis et al. 2013),
269 Interestingly, FDH is likely involved in the regulation of the extent of the root colonization by
270 WCS417, as the WCS417 colonization index is, in *atfdh1-5* roots, slightly higher than in wt ones.
271 Our proteome analysis unveils that WCS417 not only affects the production of plant proteins involved
272 in essential metabolic processes but that the plastids, and in particular several photosynthesis-related
273 proteins, are early targets of WCS417, regardless of the genetic background of the plant. These
274 findings are particularly intriguing, as the link between plant-microbial pathogens interactions and
275 chloroplasts has been already uncovered (Littlejohn et al. 2020; Yang et al. 2021), whereas the link
276 between chloroplasts and plant-beneficial bacteria was unexplored so far. Our results suggest that
277 WCS417-induces rearrangements of PSI and PSII composition, caused by reduced accumulation of
278 their proteins PSBO2, PSBP1, PSB27-1, PSAE1, and PSAE2. The physiological relevance of the
279 WCS417-induced modulation of composition, stability, and turnover of photosystems should be the
280 object of future investigations, in light of the role of chloroplasts in the biosynthesis of
281 phytohormones such as JA (Wasternack and Hause, 2019) and of previous findings suggesting that
282 WCS417 stimulates the expression of genes important for plant growth (Wintermans et al. 2016;
283 Zamioudis et al. 2013).

284 Notably, an increase in the enzymes responsible for ROS detoxification, such as glutathione S-
285 transferases (GSTs) could be observed, in both wt and *atfdh1-5* lines, upon WCS417 exposure
286 (Gullner et al. 2018). GST gene induction or increased GST activity has been reported in plants that
287 interact with beneficial bacteria (Kandasamy et al. 2009). GST7 and GST8 are upregulated in both
288 plant lines after WCS417 exposure; one possible explanation is that WCS417 triggers a temporary
289 antioxidant response, as supported by the DAB staining of the leaves exposed to WCS417, which
290 appear to accumulate less H₂O₂ than mock controls.

291 The lipoxygenase LOX2, responsible for JA synthesis (Yang et al. 2020), is one of the WCS417-
292 upregulated proteins in wt leaves. JA is involved in plant development and, along with other
293 lipoxygenases, is important during defense responses against biotic stress (Singh et al. 2022).
294 Moreover, LOX2 possesses a versatile enzymatic function as it is also essential for the biosynthesis
295 of a group of C6 aliphatic aldehydes, alcohols, and esters known as Green Leaf Volatiles GLV and
296 involved in plant defense (Mochizuki et al. 2016).

297 GSTF2, GSTF7, and LOX2 proteins were found upregulated and PSAE1 downregulated, in shoots
298 of *A. thaliana* exposed to Fe-deficient growth conditions (Zargar et al. 2013). This suggests that such
299 proteins, also identified in the present proteomic work and with a regulation similar to that described
300 by Zargar et al. (2013), might represent nodes of convergence between Fe-deficiency and WCS417-
301 induced responses in the aerial parts of the plants.

302 We also noticed differences in the response triggered by WCS417 exposure in wt and *atfdh1-5*. The
303 antioxidant enzyme APX1 is upregulated in the *atfdh1-5* mutant, in both experimental conditions
304 (mock or *P. simiae*-treated) with respect to the wt. This, in turn, might imply that *atfdh1-5* is in an
305 'alert state' with respect to the stress response. Both ROS and antioxidants are linked to salicylic acid
306 (SA) signaling (Saleem et al. 2021) and the accumulation of SA and the expression of pathogenesis-
307 related proteins are linked to the defense response Systemic Acquired Resistance (SAR) (Vallad and
308 Goodman, 2004; Vlot et al. 2021). PR5 is considered a marker for SAR triggering (Sharon et al. 2011)
309 and, surprisingly, we discovered that this protein is increased in *atfdh1-5* leaves in mock condition.

310 In the WCS417-treated *atfdh1-5* leaf proteome, several dehydrins were downregulated (HIRD11,
311 COR15B, COR47, ERD14, and ERD10). In fact, the levels of several members of this protein family
312 increased when *A. thaliana* was exposed to beneficial microorganisms which colonized its roots for
313 defense (Baek et al. 2020; Kovacs et al. 2008; Liu et al. 2020). Last, LOX2 is not upregulated in
314 *atfdh1-5* WCS417- treated leaves. Taken together, these results suggest that the lack of FDH function
315 in the *atfdh1-5* mutant alters systemic defense mechanisms in leaves, particularly after WCS417
316 treatment. FDH protein levels indeed increase in wt leaves exposed to WCS417, corroborating our
317 results on FDH promoter activity induction in *A. thaliana* leaves exposed to the rhizobacterium as
318 well as FDH involvement in an early leaf defense response against pathogens (Marzorati et al. 2021).
319 Overall, our findings on the *atfdh1-5* leaf proteome suggest that the FDH may have a relevant role in
320 the early WCS417-induced responses.

321 In conclusion, the results presented in this work can stimulate further investigations for a better
322 understanding of the signaling pathways triggered, at the foliar level, by growth-promoting
323 rhizobacteria that enhance plant resistance to environmental challenges, such as nutritional stress and
324 pathogen infections.

325

326

327

328 **Materials and methods**

329 *Plant growth*

330 *Arabidopsis thaliana* wild type Col, *atfdh1-5* mutant (Choi et al. 2014; Murgia et al. 2020), and *Vu*
331 FDH::GUS (Lou et al. 2016; Murgia et al. 2020) were stratified at 4°C and grown on Technic n.1
332 DueEmme soil by using the Arasystem (Betatech BVBA, Ghent, Belgium), *i.e.*, the Aratrays and the
333 Arabaskets, in a greenhouse at 23°C and 150 $\mu\text{E m}^{-2}\text{s}^{-1}$, with a 12 h/12 h light/dark photoperiod. *Vu*
334 FDH::GUS seeds were surface sterilized as described (van Wees et al. 2013), maintained in the dark
335 for 3 days at 4°C, then transferred on square plates dishes (100x100x20 mm, Sarstedt, Australia Ltd)
336 containing ½ MS medium supplemented with 1% sucrose, and maintained vertically in a plant growth
337 chamber at 22-25°C, 16 h/8 h light/dark photoperiod.

338

339 *Bacterial growth*

340 The *Xanthomonas campestris* pv. *campestris* (*Xcc*) strain 8004 $\Delta xopAC$ (Guy et al., 2013) was grown
341 on MOKA-rich medium (Blanvillain et al. 2007) at 28°C. Rifampicin was used at 50 $\mu\text{g ml}^{-1}$. The
342 *Pseudomonas simiae* WCS417 bacterial strain was grown overnight at 28°C on King's B medium
343 agar supplemented with 50 $\mu\text{g ml}^{-1}$ rifampicin, suspended in 10 ml of 10 mM MgSO_4 , and centrifuged
344 for 5 min at 3200 g; the pellet was washed twice in 10 mM MgSO_4 , with a 5 min centrifugation at
345 3200 g (Wintermans et al. 2016). The cell density was adjusted to 2×10^6 or 10^8 CFU ml^{-1} in 10 mM
346 MgSO_4 .

347

348 *Pathogenicity assays*

349 *A. thaliana* plants were grown in short days (8h light/16 h dark) at 22°C (60% relative humidity, 125
350 $\mu\text{E m}^{-2}\text{s}^{-1}$) for 4 weeks. Inoculations were performed as previously described (Meyer et al. 2005).
351 Fully expanded leaves were wound-inoculated by piercing three times the central vein (from the
352 middle to the tip of the leaf) with a needle dipped in a bacterial suspension at 10^8 CFU ml⁻¹ in 1 mM
353 MgCl₂. Disease development was scored using the following disease index: 0: no symptom; 1:
354 chlorosis at the inoculation point; 2: extended chlorosis; 3: necrosis; 4: leaf death.

355

356 *Plant exposure to WCS417*

357 Plants grown in soil: 1 ml of 10^8 CFU ml⁻¹ bacterial suspension, or 1 ml of 10 mM MgSO₄ (mock
358 condition), was pipetted into each Arabasket containing single 4 weeks old plants with equal
359 distribution of the liquid around the plant roots. To optimize an even distribution of the bacterial
360 inoculum for each single-root apparatus, plants were not watered for 2 days before treatment, so that
361 the Aratrays remained dry before and after inoculation. The trays, closed with transparent lids without
362 holes, were then maintained at 25°C. Seedlings grown *in vitro*: 7 days old seedlings grown on MS
363 were exposed to WCS417 avoiding any direct contact between seedlings and bacteria, as previously
364 described (Wintermans et al. 2016). Briefly, 240 μl of 2×10^6 CFU ml⁻¹ WCS417 suspension (or 240
365 μl of 10 mM MgSO₄ for mock treatment) was pipetted onto the MS medium, approximately 5 cm
366 below the seedling roots. The plates were briefly dried under laminar flow, closed with a lid and two
367 layers of parafilm, and placed again vertically in a growth chamber for two or seven days.

368

369 *WCS417 root colonization assay*

370 The assay was performed according to Stringlis et al. (2018b). In detail: *A. thaliana* wt Col and *atfdh1-*
371 5 seeds were soaked in 0.1% Tween 20 for 30 min, sterilized for 90 s in 50% commercial bleach, and
372 then rinsed thoroughly 6x with sterile distilled water. wt Col and *atfdh1-5* seeds were then plated on
373 $\frac{1}{2}$ MS square plates (10 cm x 10 cm), around 30 seeds/line, both lines in each plate, and then
374 maintained vertically in a growth chamber at 22-25°C, 16 h/8 h light/dark photoperiod.

375 After 13 days, 100 μl of a freshly prepared WCS417 suspension (10^7 CFU ml^{-1}) were evenly
376 distributed at the bottom of the hypocotyl of each seedlings line under sterility. Plates were then
377 allowed to dry and maintained again in a vertical position in the growth chamber. After 2 more days,
378 roots were cut with a sharp sterile blade at the root base, and the root samples were inserted into a 1.5
379 ml Eppendorf tube of known weight; root samples were weighed again and 1 ml 10 mM MgSO_4 was
380 then added in each tube. After 1 min vortexing, a series of bacterial dilutions was prepared from 10^0
381 (initial suspension) to 10^{-8} in 10 mM MgSO_4 ; such dilutions were plated on King's B medium agar
382 supplemented with 50 $\mu\text{g ml}^{-1}$ rifampicin and plates were maintained overnight at 28°C. Colonies
383 were then counted and CFU gr^{-1} for each sample was calculated as (colony number $\times 10 \times$ dilution
384 fold)/ root fresh weight.

385

386 *Leaves staining*

387 GUS staining: leaves and seedlings were surface-sterilized by immersion in 70% EtOH and washed
388 twice with sterile water as described (van Hulten et al. 2019). Staining for β -glucuronidase (GUS)
389 activity was performed according to Elorza et al. (2004). DAB staining: H_2O_2 staining with 3,3'-
390 diaminobenzidine (DAB) was performed as described (Murgia et al. 2004).

391

392 *Protein extraction from leaves*

393 Rosette leaves were sampled from 4 weeks old plants after 2 days of exposure to either WCS417 or
394 mock treatment, as described above. In detail, the rosette leaves from one single plant were sampled,
395 weighed (0.15-0.4 g each), packed in alufoil, frozen in liquid nitrogen, stored at -80°C, and total
396 proteins were then extracted essentially according to the protocol published by Wu et al. (2014),
397 omitting the TCA/acetone precipitation steps (steps 2-9 in the Wu et al. protocol). As starting material
398 for each extraction representing a biological sample, leaves from two different rosettes were used.
399 The protein pellets were maintained at -80°C. Pellets were then resuspended in up to 100-120 μl final
400 volume of 10 mM PBS by heating for 15 min at 37°C and vortexing, followed by 2 min centrifugation

401 at 15000 g; the supernatant contained the solubilized proteins, and if a remaining pellet could still be
402 observed, it was heated, vortexed, and centrifuged again, for one or two more cycles, for thorough
403 solubilization of all the proteins in the starting frozen pellet.

404

405 *Enzymatic digestion of protein extracts*

406 The total protein extract of each sample was concentrated from 100 to 50 μl in a vacuum concentrator
407 at 60 °C and treated with 0.25% (w/v) RapiGestTMSF reagent (Waters Co, Milford, MA, USA). The
408 resulting suspensions were incubated with stirring at 100°C for 20 min, cooled to RT, and centrifuged
409 for 10 min at 2200 g. The protein concentration was assayed using the InvitrogenTM QubitTM Protein
410 BR Assay Kit (Life Technologies Corporation, Thermo Fisher, Eugene, ORE, USA), and 50 μg of
411 protein from each sample was digested overnight at 37°C by adding Sequencing-grade Modified
412 Trypsin (Promega Inc., Madison, WI, USA) at a 1:50 (w/w) enzyme/substrate ratio. An additional
413 aliquot of trypsin (1:100 w/w) was then added in the morning, and the digestion continued for 4h.
414 The enzymatic digestion was chemically stopped by acidification with 0.5% Trifluoroacetic Acid
415 (TFA) (Sigma-Aldrich Inc., St.Louis, MO, USA) and a subsequent incubation at 37°C for 45 min
416 completed the RapiGest acid hydrolysis. Water-immiscible degradation products were removed by
417 centrifugation at 13000 rpm for 10 min. Finally, the tryptic digest mixtures were desalted using
418 PierceTM C-18 spin columns (Thermo Fisher Scientific, Pierce Biotechnology, Rockford, IL, USA),
419 according to manufacturer protocol and were resuspended in 0.1% formic acid (Sigma-Aldrich Inc.,
420 St. Louis, MO, USA) in water (LC-MS Ultra CHROMASOLVTM, Honeywell Riedel-de HaenTM,
421 Muskegon, MI, USA) at a concentration of 0.2 $\mu\text{g } \mu\text{l}^{-1}$.

422

423 *LC-MS/MS Analysis*

424 Peptide mixtures were analyzed using Eksigent nanoLC-Ultra® 2D System (Eksigent, part of AB
425 SCIEX Dublin, CA, USA) configured in trap-elute mode. Briefly, samples (0.8 μg injected) were
426 first loaded on a trap (200 μm x 500 μm ChromXP C18-CL, 3 μm , 120 Å) and washed with the

427 loading pump running in isocratic mode with 0.1% formic acid in water for 10 min at a flow of 3 μL
428 min^{-1} . The automatic switching of the autosampler ten-port valve then eluted the trapped mixture on
429 a nano reversed-phase column (75 μm x 15 cm ChromXP C18-CL, 3 μm , 120 \AA) through a 145 min
430 gradient of eluent B (eluent A, 0.1% formic acid in water; eluent B, 0.1% formic acid in acetonitrile)
431 at a flow rate of 300 nl min^{-1} . In-depth, the gradient was: from 5-10% B in 3 min, 10-30% B in 104
432 min, 30-95% B in 26 min, and holding at 95% B for 12 min. The eluted peptides were directly
433 analyzed on an LTQ-OrbitrapXL mass spectrometer (Thermo Fisher Scientific, CA, USA) equipped
434 with a nanospray ion source. The spray capillary voltage was set at 1.7 kV and the ion transfer
435 capillary temperature was held at 220°C. Full MS spectra were recorded over a 400–1600 m/z range
436 in positive ion mode, with a resolving power of 60000 (full width at half-maximum) and a scan rate
437 of 2 spectra s^{-1} . This step was followed by five low-resolution MS/MS events that were sequentially
438 generated in a data-dependent manner on the top five ions selected from the full MS spectrum (at
439 35% collision energy) using dynamic exclusion of 0.5 min for MS/MS analysis. Mass spectrometer
440 scan functions and high-performance liquid chromatography solvent gradients were controlled by the
441 Xcalibur data system version 1.4 (Thermo Fisher Scientific, CA, USA).

442

443 *LC-MS/MS spectra processing and data handling*

444 The Proteome Discoverer software 2.5 using SEQUEST HT search engine (Thermo Fisher Scientific,
445 San José, CA, USA) was used to process all LC-MS/MS runs against *Arabidopsis thaliana* counting
446 39256 entries (www.uniprot.org, downloaded in July 2022). The following criteria were used for
447 peptide and related protein identification: trypsin as enzyme with 2 missed cleavage per peptide, mass
448 tolerance of ± 50 ppm mass tolerance for the precursor, and ± 0.8 Da for fragment ions. Validation
449 was performed by Percolator node with a target-decoy search and a false discovery rate (FDR) ≤ 0.01
450 and maximum deltaCN of 0.05. The minimum peptide length of 7 amino acids at confidence
451 ‘Medium’ level was set. Peptide Spectral Matches (PSMs) were used in a label-free quantification
452 approach to compare protein lists ($n=24$) and identify proteins differentially expressed (DEPs), as

453 previously reported (Palma et al. 2021). Briefly, data matrix complexity was reduced by linear
 454 discriminant analysis (LDA) and in a pairwise comparison (wt Col mock-treated vs wt Col WCS417-
 455 treated; *atfdh1-5* mock-treated vs *atfdh1-5* WCS417-treated; wt Col mock-treated vs *atfdh1-5* mock-
 456 treated; wt Col WCS417-treated vs *atfdh1-5* WCS417-treated) and proteins with $P \leq 0.05$ were
 457 retained. Pairwise comparisons were further evaluated by DAve index $((\text{PSMs}_A - \text{PSMs}_B) / (\text{PSMs}_A + \text{PSMs}_B)) / 0.5$, where A and B represent the samples compared; specifically,
 458 positive DAve values indicate proteins upregulated in A (and downregulated in B), while negative
 459 DAve values indicate proteins upregulated in B (and downregulated in A) (Mauri and Dehò, 2008).
 460 Finally, DEPs were processed by hierarchical clustering using Ward's method and the Euclidean
 461 distance metric. All data processing was performed by JMP15.2 SAS. Using STRING Cytoscape's
 462 APP (Doncheva et al. 2019), the protein profile characterized for wt Col mock-treated, wt Col
 463 WCS417-treated, *atfdh1-5* mock-treated, and *atfdh1-5* WCS417-treated phenotypes were evaluated
 464 at the functional level, and the most enriched KEGG pathways and biological processes were
 465 extracted and compared (wt Col mock-treated vs wt WCS417-treated; *atfdh1-5* mock-treated vs
 466 *atfdh1-5* WCS417-treated; wt Col mock-treated vs *atfdh1-5* mock-treated; wt Col WCS417-treated
 467 vs *atfdh1-5* WCS417) by unpaired t-test ($P \leq 0.01$).

469

470 *Statistical analysis*

471 To test for significant differences between WCS417-treated plants and mock-treated plants for the *in*
 472 *vivo* data experiments, an unpaired t-test was run, establishing for each comparison equal or unequal
 473 variances before the analysis by an F-test two samples for variances. In detail: for *in vitro* mock-
 474 treated two days (sample size: 54) vs *in vitro* WCS417-treated two days (sample size: 63) unequal
 475 variances were assumed, $P = 0.04512639$ ($P < 0.05$); for *in vitro* mock-treated seven days (sample
 476 size: 70) vs *in vitro* WCS417-treated seven days (sample size: 135) equal variances were assumed, P
 477 $= 3.052E^{-08}$ ($P < 0.01$); for *in vivo* mock-treated two days (sample size: 36) vs *in vivo* WCS417-treated
 478 two days (sample size: 36) equal variances were assumed, $P = 0.001576$ ($P < 0.01$); for *in vivo* mock-

479 treated four days (sample size: 82) vs *in vivo* WCS417-treated four days (sample size: 100) unequal
480 variances were assumed, $P = 0.01385$ ($P \leq 0.01$); for close to mock (sample size: 90) vs close to
481 WCS417 (sample size: 99) equal variances were assumed, $P = 0.4325$ (not statistically significant);
482 for Col mock-treated weights (sample size: 25) vs Col WCS417-treated weights (sample size: 25)
483 unequal variances were assumed, $P = 0.002381$ ($P < 0.01$); for *atfdh1-5* mock-treated weights (sample
484 size: 25) vs *atfdh1-5* WCS417-treated weights (sample size: 25) unequal variances were assumed, P
485 = 0.0002032 ($P < 0.01$); for the WCS417 colonization test (sample size: ~ 30) equal variances were
486 assumed, $P = 0.039$ ($P < 0.05$). All data processing was performed by using R (ver. 4.1.0), packages
487 *ggpubr* and *dplyr*.

488

489 *Photochemical parameters*

490 The photochemical parameters F_0 , F_m , F_v , and maximal photochemical efficiency F_v/F_m were
491 measured in dark-adapted leaves (20 min) as previously described (Murgia et al. 2020).

492

493

494 **Acknowledgments**

495 We are grateful to Peter Bakker for donating the *Pseudomonas simiae* WCS417 strain. This work was
496 supported by the Italian National Ministry of Research (MIUR) (2017-2017FBS8YN_00 (DD)
497 PRIN); it was also supported by a grant from the Agence Nationale de la Recherche NEPHRON
498 project (ANR-18-CE20-0020-01) to EL and LDN. This study is set within the framework of the
499 ‘Laboratoires d’Excellences’ (LABEX) TULIP (ANR-10-LABX-41) and of the ‘Ecole Universitaire
500 de Recherche’ (EUR) TULIP-GS (ANR-18-EURE-0019).

501 PM acknowledges the support of the APC central fund of the University of Milano.
502

503

504 **Authors contributions**

505 FM, IM, and PM conceived the experiments; FM and IM performed the *in vitro* and *in vivo*
506 experiments, with contributions from PM; EL and LDN performed the pathogenic assay with *Xcc*;
507 DDS, RR, LB, and PLM performed the proteomic analysis; FM, PM, IM, DDS, LB, EL and LDN
508 analyzed the results; FM, IM, and PM wrote the manuscript. All authors agreed to the final version
509 of the manuscript.

510

511 **Literature cited**

- 512 Alekseeva, A. A., Savin, S. S., and Tishkov, V. I. 2011. NAD⁺-dependent formate dehydrogenase from
513 plants. *Acta Nat.* 3:38-54.
- 514 Ali, S., Ahmad Ganai, B., Kamili, A. N., Ali Bhat, A., Ahmad Mir, Z., Akhter Bhat, J., Tyagi, A.,
515 Tajamul Islam, S., Mushtaq, M., Yadav, P., Rawat, S., and Grover, A. 2018. Pathogenesis-related
516 proteins and peptides as promising tools for engineering plants with multiple stress tolerance,
517 *Microbiol. Res.* 212:29-37.
- 518 Ambard-Bretteville, F., Sorin, C., Rébeillé, F., Hourton-Cabassa, C., and Colas Des Francs-Small, C.
519 2003. Repression of formate dehydrogenase in *Solanum tuberosum* increases steady-state levels of
520 formate and accelerates the accumulation of proline in response to osmotic stress. *Plant Mol. Biol.*
521 52:1153-1168.
- 522 Ambrosone, A., Batelli, G., Nurcato, R., Aurilia, V., Punzo, P., Bangarusamy, D. K., Ruberti, I., Sassi,
523 M., Leone, A., Costa, A., and Grillo, S. 2015. The *Arabidopsis* RNA-binding protein AtRGGA
524 regulates tolerance to salt and drought stress. *Plant Physiol.* 168:292-306.
- 525 Andreadeli, A., Fletmetakis, E., Axarli, I., Dimou, M., Udvardi, M. K., Katinakis, P., and Labrou, N. E.
526 2009. Cloning and characterization of *Lotus japonicus* formate dehydrogenase: a possible
527 correlation with hypoxia. *Biochim. Biophys. Acta. Proteins and Proteomes* 1794:976-984.
- 528 Baek, D., Rokibuzzaman, M., Khan, A., Kim, M. C., Park, H. J., Yun, D. J., and Chung, Y. R. 2020.
529 Plant-growth promoting *Bacillus oryzicola* YC7007 modulates stress-response gene expression
530 and provides protection from salt stress. *Front. Plant Sci.* 10:1646.
- 531 Berendsen, R.L., van Verk, M.C., Stringlis, I.A. *et al.* 2015. Unearthing the genomes of plant-beneficial
532 *Pseudomonas* model strains WCS358, WCS374 and WCS417. *BMC Genom.* 16:539.
- 533 Blanvillain S, Meyer D, Boulanger A, Lautier M, Guynet C, Denancé N, et al. 2007. Plant carbohydrate
534 scavenging through TonB-Ddependent receptors: A feature shared by phytopathogenic and aquatic
535 bacteria. *PLoS ONE.* 2:e224.

- 536 Chen, Y. E., Zhao, Z. Y., Zhang, H. Y., Zeng, X. Y., and Yuan, S. 2013. Significance of CP29 reversible
537 phosphorylation in thylakoids of higher plants under environmental stresses. *J. Exp. Bot.* 64:1167-
538 1178.
- 539 Choi, D. S., Kim, N. H., and Hwang, B. K. 2014. Pepper mitochondrial formate dehydrogenase1
540 regulates cell death and defense responses against bacterial pathogens. *Plant Physiol.* 166:1298-
541 1311.
- 542 Cormann, K. U., Möller, M., and Nowaczyk, M. M. 2016. Critical assessment of protein cross-linking
543 and molecular docking: An updated model for the interaction between photosystem II and Psb27.
544 *Front. Plant Sci.* 7:157.
- 545 David, P., Colas Des Francs-Small, C., Sévignac, M., Thareau, V., Macadré, C., Langin, T., and Geffroy,
546 V. 2010. Three highly similar formate dehydrogenase genes located in the vicinity of the B4
547 resistance gene cluster are differentially expressed under biotic and abiotic stresses in *Phaseolus*
548 *vulgaris*. *Theor. Appl. Genet.* 121:87-103.
- 549 Desrut, A., Moumen, B., Thibault, F., Le Hir, R., Coutos-Thévenot, P., and Vriet C. 2020. Beneficial
550 rhizobacteria *Pseudomonas simiae* WCS417 induce major transcriptional changes in plant sugar
551 transport. *J Exp Bot.* 71:7301-7315.
- 552 De Weert, S., Vermeiren, H., Mulders, I. H. M., Kuiper, I., Hendrickx, N., Bloemberg, G. V.,
553 Vanderleyden, J., de Mot, R., and Lugtenberg, B. J. J. 2002. Flagella-driven chemotaxis towards
554 exudate components is an important trait for tomato root colonization by *Pseudomonas fluorescens*.
555 *Mol. Plant Microbe Interact.* 15:1173-1180.
- 556 Dietz, K. J., Tavakoli, N., Kluge, C., Mimura, T., Sharma, S. S., Harris, G. C., Chardonnens, A. N., and
557 Gollmack, D. 2001. Significance of the V-type ATPase for the adaptation to stressful growth
558 conditions and its regulation on the molecular and biochemical level. *J. Exp. Bot.* 52:1969-1980.
- 559 Di Silvestre, D., Vigani, G., Mauri, P., Hammadi, S., Morandini, P., and Murgia, I. 2021. Network
560 topological analysis for the identification of novel hubs in plant nutrition. *Front. Plant Sci.* 12:
561 629013.

- 562 Doncheva, N. T., Morris, J. H., Gorodkin, J., and Jensen, L. J. 2019. Cytoscape StringApp: Network
563 analysis and visualization of proteomics data. *J. Proteome Res.* 18:623-632.
- 564 Elorza, A., León, G., Gómez, I., Mouras, A., Holuigue, L., Araya, A., and Jordana, X. 2004. Nuclear
565 SDH2-1 and SDH2-2 genes, encoding the iron-sulfur subunit of mitochondrial complex II in
566 *Arabidopsis*, have distinct cell-specific expression patterns and promoter activities. *Plant Physiol.*
567 136:4072-4087.
- 568 Gullner, G., Komives, T., Király, L., and Schröder, P. 2018. Glutathione S-transferase enzymes in plant-
569 pathogen interactions. *Front. Plant Sci.* 9:1836.
- 570 Guy, E., Lautier, M., Chabannes, M., Roux, B., Lauber, E., Arlat, E., Noël, L.D. 2013. xopAC-triggered
571 immunity against *Xanthomonas* depends on *Arabidopsis* receptor-like cytoplasmic kinase genes
572 PBL2 and RIPK. *PLoS ONE* 8:e73469.
- 573 Herman, P. L., Ramberg, H., Baack, R. D., Markwell, J., and Osterman, J. C. 2002. Formate
574 dehydrogenase in *Arabidopsis thaliana*: Overexpression and subcellular localization in leaves.
575 *Plant Sci.* 163:1137-1145.
- 576 Hong, X., Qi, F., Wang, R., Jia, Z., Lin, F., Yuan, M., Xin, X., and Liang, Y. 2022. Ascorbate peroxidase
577 1 allows monitoring of cytosolic accumulation of effector-triggered reactive oxygen species using
578 a luminol-based assay. *Plant Physiol.* 191:1416-1434.
- 579 Hourton-Cabassa, C., Ambard-Bretteville, F., Moreau, F., de Virville, J.D., Rémy, R., and Colas Des
580 Francs-Small, C. 1998. Stress induction of mitochondrial formate dehydrogenase in potato leaves.
581 *Plant Physiol.* 116:627-635.
- 582 Huang, J. B., Zou, Y., Zhang, X., Wang, M., Dong, Q., and Tao, L. Z. 2020. RIBOSE PHOSPHATE
583 ISOMERASE 1 influences root development by acting on cell wall biosynthesis, actin
584 organization, and auxin transport in *Arabidopsis*. *Front. Plant Sci.* 10:1641.
- 585 Jin, C. W., He, Y.F., Tang, C. X., Wu, P., and Zheng, S. J. 2006. Mechanisms of microbially enhanced
586 Fe acquisition in red clover (*Trifolium pratense* L.). *Plant Cell Environ.* 29:888-897.

- 587 Jin, C. W., Li, G. X., Yu, X. H., and Zheng, S. J. 2010. Plant Fe status affects the composition of
588 siderophore-secreting microbes in the rhizosphere. *Ann. Bot.* 105:835-841.
- 589 Kandasamy, S., Loganathan, K., Muthuraj, R., Duraisamy, S., Seetharaman, S., Thiruvengadam, R.,
590 Ponnusamy, B., and Ramasamy, S. 2009. Understanding the molecular basis of plant growth
591 promotional effect of *Pseudomonas fluorescens* on rice through protein profiling. *Proteome Sci.*
592 7:47.
- 593 Kovacs, D., Kalmar, E., Torok, Z., and Tompa, P. 2008. Chaperone activity of ERD10 and ERD14, two
594 disordered stress-related plant proteins. *Plant Physiol.* 147:381-390.
- 595 Kurt-Gür, G., Demirci, H., Sunulu, A., and Ordu, E. 2018. Stress response of NAD⁺-dependent formate
596 dehydrogenase in *Gossypium hirsutum* L. grown under copper toxicity. *Environ. Sci. Pollut. Res.*
597 25:31679-31690.
- 598 Kushwaha, R., Singh, A., and Chattopadhyay, S. 2008. Calmodulin7 plays an important role as
599 transcriptional regulator in *Arabidopsis* seedling development. *Plant Cell* 20:1747-1759.
- 600 Lee, S., Vemanna, R. S., Oh, S., Rojas, C. M., Oh, Y., Kaundal, A., Kwon, T., Lee, H. K., Senthil-
601 Kumar, M., and Mysore, K. S. 2022. Functional role of formate dehydrogenase 1 (FDH1) for host
602 and nonhost disease resistance against bacterial pathogens. *PloS ONE.* 17:e0264917.
- 603 Li, R., Moore, M., Bonham-Smith, P. C., and King, J. 2002. Overexpression of formate dehydrogenase
604 in *Arabidopsis thaliana* resulted in plants tolerant to high concentrations of formate. *J. Plant*
605 *Physiol.* 159:1069-1076.
- 606 Li, Y., Zeng, H., Xu, F., Yan, F., and Xu, W. 2022. H⁺-ATPases in plant growth and stress responses.
607 *Annu. Rev. Plant Biol.* 73:495-521.
- 608 Littlejohn, G. R., Breen, S., Smirnoff, N., and Grant, M. 2020. Chloroplast immunity illuminated. *New*
609 *Phytol.* 229:3088-3107.
- 610 Liu, W., Sikora, E., and Park, S. W. 2020. Plant growth-promoting rhizobacterium, *Panebacillus*
611 *polymyxa* CR1, upregulates dehydration-responsive genes, RD29A and RD29B, during priming
612 drought tolerance in *Arabidopsis*. *Plant Physiol. Biochem.* 156:146-154.

- 613 Lou, H. Q., Gong, Y. L., Fan, W., Xu, J. M., Liu, Y., Cao, M. J., Wang, M. H., Yang, J. L., and Zheng,
614 S. J. 2016. A formate dehydrogenase confers tolerance to aluminum and low pH. *Plant Physiol.*
615 171:294-305.
- 616 Lundin, B., Hansson, M., Schoefs, B., Vener, A. V., and Spetea, C. 2007. The *Arabidopsis* PsbO2
617 protein regulates dephosphorylation and turnover of the photosystem II reaction centre D1 protein.
618 *Plant J.* 49:528-539.
- 619 Ma, B., Qian, D., Nan, Q., Tan, C., An, L., and Xiang, Y. 2012. *Arabidopsis* vacuolar H⁺-ATPase (V-
620 ATPase) B subunits are involved in actin cytoskeleton remodeling via binding to, bundling, and
621 stabilizing F-actin. *J. Biol. Chem.* 287:19008-19017.
- 622 Marzorati, F., Vigani, G., Morandini, P., and Murgia, I. 2021. Formate dehydrogenase contributes to the
623 early *Arabidopsis thaliana* responses against *Xanthomonas campestris* pv *campestris* infection.
624 *Physiol. Mol. Plant Pathol.* 114:101633.
- 625 Mauri, P., and Dehò, G. 2008. A proteomic approach to the analysis of RNA degradosome composition
626 in *Escherichia coli*. *Methods Enzymol.* 447:99-117.
- 627 Meyer, D., Lauber, E., Roby, D., Arlat, M., and Kroj, T. 2005. Optimization of pathogenicity assays
628 to study the *Arabidopsis thaliana*-*Xanthomonas campestris* pv. *Campestris* pathosystem. *Mol. Plant*
629 *Pathol.* 6:327-33.
- 630 Mochizuki, S., Sugimoto, K., Koeduka, T., and Matsui, K. 2016. *Arabidopsis* lipoxygenase 2 is
631 essential for formation of green leaf volatiles and five-carbon volatiles. *FEBS Lett.* 590:1017-1027.
- 632 Murgia, I., Tarantino, D., Vannini, C., Bracale, M., Carravieri, S., and Soave, C. 2004. *Arabidopsis*
633 *thaliana* plants overexpressing thylakoidal ascorbate peroxidase show increased resistance to
634 Paraquat-induced photooxidative stress and to nitric oxide-induced cell death. *Plant J.* 38:940-953.
- 635 Murgia, I., Vigani, G., Di Silvestre, D., Mauri, P., Rossi, R., Bergamaschi, A., Frisella, M., and
636 Morandini, P. 2020. Formate dehydrogenase takes part in molybdenum and iron homeostasis and
637 affects dark-induced senescence in plants. *J. Plant Interact.* 15:386-397.

- 638 Olson, B. J., Skavdahl, M., Ramberg, H., Osterman, J.C., and Markwell, J. 2000. Formate
639 dehydrogenase in *Arabidopsis thaliana*: characterization and possible targeting to the chloroplast.
640 Plant Sci. 159:205-212.
- 641 Pagnussat, G. C., Yu, H. J., Ngo, Q. A., Rajani, S., Mayalagu, S., Johnson, C. S., Capron, A., Xie, L. F.,
642 Ye, D., and Sundaresan, V. 2005. Genetic and molecular identification of genes required for female
643 gametophyte development and function in *Arabidopsis*. Development. 132:603-614.
- 644 Palma, C., la Rocca, C., Gigantino, V., Aquino, G., Piccaro, G., Di Silvestre, D., Brambilla, F., Rossi,
645 R., Bonacina, F., Lepore, M. T., Audano, M., Mitro, N., Botti, G., Bruzzaniti, S., Fusco, C.,
646 Procaccini, C., de Rosa, V., Galgani, M., Alviggi, C., Puca, A., Grassi, F., Rezzonico-Jost, T.,
647 Norata, G. D., Mauri, P., Netea, M. G., de Candia, P., and Matarese, G. 2021. Caloric restriction
648 promotes immunometabolic reprogramming leading to protection from tuberculosis. Cell Metab.
649 33:300-318.
- 650 Palmer, C. M., Hindt, M. N., Schmidt, H., Clemens, S., and Guerinot, M. L. 2013. MYB10 and MYB72
651 are required for growth under iron-limiting conditions. PLoS Genet. 9:e1003953.
- 652 Pieterse, C. M. J., Berendsen, R. L., de Jonge, R., and Stringlis, I. A. 2020. *Pseudomonas simiae*
653 WCS417: star track of a model beneficial rhizobacterium. Plant Soil. 461:245-263.
- 654 Romera, F. J., García, M. J., Lucena, C., Martínez-Medina, A., Aparicio, M. A., Ramos, J., Alcántara,
655 E., Angulo, M., and Pérez-Vicente, R. 2019. Induced systemic resistance (ISR) and Fe deficiency
656 responses in dicot plants. Front Plant Sci. 10:287.
- 657 Saleem, M., Fariduddin, Q., and Castroverde, C. D. M 2021. Salicylic acid: a key regulator of redox
658 signalling and plant immunity. Plant Physiol. Biochem. 168:381-397.
- 659 Sappl, P. G., Oñate-Sánchez, L., Singh, K. B., and Millar, A. H. 2004. Proteomic analysis of glutathione
660 S-transferases of *Arabidopsis thaliana* reveals differential salicylic acid-induced expression of the
661 plant-specific phi and tau classes. Plant Mol. Biol. 54:205-219.
- 662 Sasaki, K., Kim, M.H., and Imai, R. 2013. *Arabidopsis* COLD SHOCK DOMAIN PROTEIN 2 is a
663 negative regulator of cold acclimation. New Phytol. 198:95-102.

- 664 Sharon, M., Freeman, S., and Sneh, B. 2011. Assessment of resistance pathways induced in *Arabidopsis*
665 *thaliana* by hypovirulent *Rhizoctonia* spp. isolates. *Phytopathology*. 101:828-838.
- 666 Simons, M., van der Bij, A. J., Brand, I., de Weger, L. A., Wijffelman, C. A., and Lugtenberg, B. J. J.
667 1996. Gnotobiotic system for studying rhizosphere colonization by plant growth-promoting
668 *Pseudomonas* bacteria. *Mol. Plant Microbe Interact.* 9:600-607.
- 669 Singh, P., Arif, Y., Miszczuk, E., Bajguz, A., and Hayat, S. 2022. Specific roles of lipoxygenases in
670 development and responses to stress in plants. *Plants*. 11:979.
- 671 Singh, D. K., Maximova, S. N., Jensen, P. J., Lehman, B. L., Ngugi, H. N., and McNellis, T. W. 2010.
672 FIBRILLIN4 is required for plastoglobule development and stress resistance in apple and
673 *Arabidopsis*. *Plant Physiol.* 154:1281-1293.
- 674 Stringlis, I. A., Proietti, S., Hickman, R., van Verk, M. C., Zamioudis, C., and Pieterse, C. M. J. 2018a.
675 Root transcriptional dynamics induced by beneficial rhizobacteria and microbial immune elicitors
676 reveal signatures of adaptation to mutualists. *Plant J.* 93:166-180.
- 677 Stringlis, I. A., Yu K., Feussner K., de Jonge R., Van Bentum S., Van Verk M. C., Berendsen R. L.,
678 Bakker P. A. H. M., Feussner I., Pieterse C. M. J. 2018b. MYB72-dependent coumarin exudation
679 shapes root microbiome assembly to promote plant health. *Proc. Natl. Acad. Sci. USA.* 115:E5213–
680 E5222.
- 681 Sun, Z., Li, S., Chen, W., Zhang, J., Zhang, L., Sun, W., and Wang, Z. 2021. Molecular sciences plant
682 dehydrins: Expression, regulatory networks, and protective roles in plants challenged by abiotic
683 stress. *J. Mol. Sci.* 22:12619.
- 684 Suzuki, K., Itai, R., Suzuki, K., Nakanishi, H., Nishizawa, N. K., Yoshimura, E., and Mori, S. 1998.
685 Formate dehydrogenase, an enzyme of anaerobic metabolism, is induced by iron deficiency in
686 barley roots. *Plant Physiol.* 116:725-732.
- 687 Sylvestre-Gonon, E., Law, S. R., Schwartz, M., Robe, K., Keech, O., Didierjean, C., Dubos, C., Rouhier,
688 N., and Hecker, A. 2019. Functional, structural and biochemical features of plant serinyl-
689 glutathione transferases. *Front Plant Sci.* 10:608.

- 690 Trapet, P., Avoscan, L., Klinguer, A., Pateyron, S., Citerne, S., Chervin, C., Mazurier, S., Lemanceau,
691 P., Wendehenne, D., and Besson-Bard, A. 2016. The *Pseudomonas fluorescens* siderophore
692 pyoverdine weakens *Arabidopsis thaliana* defense in favor of growth in iron-deficient conditions.
693 *Plant Physiol.* 171:675-693.
- 694 Trapet, P. L., Verbon, E. H., Bosma, R. R., Voordendag, K., van Pelt, J. A., and Pieterse, C. M. J. 2021.
695 Mechanisms underlying iron deficiency-induced resistance against pathogens with different
696 lifestyles. *J. Exp. Bot.* 72:2231-2241.
- 697 Vallad, G. E., and Goodman, R. M. 2004. Systemic acquired resistance and induced systemic resistance
698 in conventional agriculture. *Crop Sci.* 44:1920-1934.
- 699 van Hulten, M., Chatterjee, S., and van den Burg, H. A. 2019. Infection assay for *Xanthomonas*
700 *campestris* pv. *campestris* in *Arabidopsis thaliana* mimicking natural entry via hydathodes.
701 *Methods Mol. Biol.* 1991:159-185.
- 702 Verbon, E. H., Trapet, P. L., Kruijs, S., Temple-Boyer-Dury, C., Rouwenhorst, T. G., and Pieterse, C.
703 M. J. 2019. Rhizobacteria-mediated activation of the Fe deficiency response in *Arabidopsis* roots:
704 Impact on Fe status and signaling. *Front Plant Sci.* 10:909.
- 705 Vigani, G., Di Silvestre, D., Agresta, A. M., Donnini, S., Mauri, P., Gehl, C., Bittner, F., and Murgia, I.
706 2017. Molybdenum and iron mutually impact their homeostasis in cucumber (*Cucumis sativus*)
707 plants. *New Phytol.* 213:1222-1241.
- 708 Vlot, A. C., Sales, J. H., Lenk, M., Bauer, K., Brambilla, A., Sommer, A., Chen, Y., Wenig, M., and
709 Nayem, S. 2021. Systemic propagation of immunity in plants. *New Phytol.* 229:1234-1250.
- 710 Wang, H., Liu, R., You, M.P., Barbetti, M. J., and Chen, Y. 2021. Pathogen biocontrol using plant
711 growth-promoting bacteria (PGPR): Role of bacterial diversity. *Microorganisms.* 9:1988.
- 712 Wang, L., Ouyang, M., Li, Q., Zou, M., Guo, J., Ma, J., Lu, C., and Zhang, L. 2010. The *Arabidopsis*
713 chloroplast ribosome recycling factor is essential for embryogenesis and chloroplast biogenesis.
714 *Plant Mol Biol.* 74:47-59.

- 715 Wasternack, C., and Hause, B. 2019. The missing link in jasmonic acid biosynthesis. *Nat. Plants*. 5:776-
716 777.
- 717 van Wees, S. C. M., van Pelt, J. A., Bakker, P. A. H. M., and Pieterse, C. M. J. 2013. Bioassays for
718 assessing jasmonate-dependent defenses triggered by pathogens, herbivorous insects, or beneficial
719 rhizobacteria. *Methods Mol. Biol.* 1011:35-49.
- 720 Wintermans, P. C. A., Bakker, P. A. H. M., and Pieterse, C. M. J. 2016. Natural genetic variation in
721 *Arabidopsis* for responsiveness to plant growth-promoting rhizobacteria. *Plant Mol. Biol.* 90:623-
722 634.
- 723 Wu, X., Xiong, E., Wang, W., Scali, M., and Cresti, M. 2014. Universal sample preparation method
724 integrating trichloroacetic acid/acetone precipitation with phenol extraction for crop proteomic
725 analysis. *Nat. Protoc.* 9:362-374.
- 726 Yang, T. H., Lenglet-Hilfiker, A., Stolz, S., Glauser, G., and Farmer, E. E. 2020. Jasmonate precursor
727 biosynthetic enzymes LOX3 and LOX4 control wound-response growth restriction. *Plant Physiol.*
728 184:1172-1180.
- 729 Yang, F., Xiao, K., Pan, H., and Liu J. 2021. Chloroplasts: the emerging battlefield in plant-microbe
730 interactions. *Front. Plant Sci.* 12:637853.
- 731 Yi, X., Hargett, S. R., Liu, H., Frankel, L. K., and Bricker, T. M. 2007. The PsbP protein is required for
732 photosystem II complex assembly/stability and photoautotrophy in *Arabidopsis thaliana*. *J. Biol.*
733 *Chem.* 282:24833-24841.
- 734 Zamioudis, C., Mastranesti, P., Dhonukshe, P., Blilou, I., and Pieterse, C. M. J. 2013. Unraveling root
735 developmental programs initiated by beneficial *Pseudomonas* spp. bacteria. *Plant Physiol.*
736 162:304-318.
- 737 Zamioudis, C., Hanson, J., and Pieterse, C. M. J. 2014. β -Glucosidase BGLU42 is a MYB72-dependent
738 key regulator of rhizobacteria-induced systemic resistance and modulates iron deficiency responses
739 in *Arabidopsis* roots. *New Phytol.* 204:368-379.

- 740 Zamioudis, C., Korteland, J., van Pelt, J. A., van Hamersveld, M., Dombrowski, N., Bai, Y., Hanson, J.,
741 van Verk, M.C., Ling, H. Q., Schulze-Lefert, P., and Pieterse, C. M. J. 2015. Rhizobacterial
742 volatiles and photosynthesis-related signals coordinate MYB72 expression in *Arabidopsis* roots
743 during onset of induced systemic resistance and iron-deficiency responses. *Plant J.* 84:309-322.
- 744 Zargar, S. M., Kurata, R., Inaba, S., and Fukao, Y. 2013. Unraveling the iron deficiency responsive
745 proteome in *Arabidopsis* shoot by iTRAQ-OFFGEL approach. *Plant Signal. Behav.* 8:e26892.
- 746 Zhang, H., Sun, Y., Xie, X., Kim, M. S., Dowd, S. E., and Paré, P. W. 2009. A soil bacterium regulates
747 plant acquisition of iron via deficiency-inducible mechanisms. *Plant J.* 58:568-577.

748 **Table 1**

749 Proteins with increased expression in *A. thaliana* wt Col and *atfdh1-5* leaves, after root exposure to WCS417. The list of proteins identified by
750 proteomic analysis which are upregulated in the leaves of both wt Col and *atfdh1-5* after two days of root exposure to WCS417 (or to mock treatment),
751 are reported; the name, AGI code, UniProt ID, annotation, subcellular localization according to Aramemnon (<http://aramemnon.uni-koeln.de>) and
752 SUBA5 (<https://suba.live/>) (according to their respective highest scores), F ratio and Probability ($P \leq 0.01$) (by LDA), and DAve index (by MAProMa)
753 are reported. SP: secretory pathway; PM: plasma membrane.

754

755

Protein name	AGI code	UniProt ID	Annotation	Localization (Aramemnon/SUBA5)	F ratio		Prob > F		DAve	
					wt Col	<i>atfdh1-5</i>	wt Col	<i>atfdh1-5</i>	wt Col	<i>atfdh1-5</i>
EIF4A1	AT3G13920	A8MRZ7	Transl. initiation factor 4A1	nucleus/cytosol	11	19	8.0E ⁻⁰³	1.3E ⁻⁰³	-0.41	-0.79
GSTF7	AT1G02920	Q9SRY5	Glutathione S-transferase F7	mitoch/cytosol	11	15	7.6E ⁻⁰³	3.3E ⁻⁰³	-2.0	-2.0
GSTF8	AT2G47730	Q96266	Glutathione S-transferase F8	plastid/plastid	16	14	2.6E ⁻⁰³	3.7E ⁻⁰³	-0.96	-1.09
PAP6	AT3G23400	Q9LW57	Plastid-lipid-associated protein 6	plastid/plastid	16	51	2.5E ⁻⁰³	3.1E ⁻⁰⁵	-1.18	-1.60
RPI3	AT3G04790	Q9S726	Putative ribose-5-phosphate isomerase 3	plastid/plastid	15	15	3.1E ⁻⁰³	3.1E ⁻⁰³	-0.89	-0.91
RPS1	AT5G30510	Q93VC7	30S ribosomal protein S1	plastid/plastid	14	19	4.1E ⁻⁰³	1.4E ⁻⁰³	-1.16	-1.18
RPS18C	AT4G09800	P34788	40S ribosomal protein S18	mitoch/cytosol	52	29	2.9E ⁻⁰⁵	2.9E ⁻⁰⁴	-1.20	-0.53
VHA-B1	AT1G76030	P11574	V-type proton ATPase subunit B1	SP/Golgi or vacuole	22	11	8.8E ⁻⁰⁴	7.1E ⁻⁰³	-2.0	-0.95
VHA-C	AT1G12840	Q9SDS7	V-type proton ATPase subunit C	mitoch/Golgi or vacuole	35	43	1.4E ⁻⁰⁴	6.7E ⁻⁰⁵	-1.46	-1.72
atpB	ATCG00480	P19366	ATP synthase subunit beta	/plastid	18	13	1.8E ⁻⁰³	4.9E ⁻⁰³	-0.28	-0.20

756

757 **Table 2**

758 Proteins with decreased expression in *A. thaliana* wt Col and *atfdh1-5* leaves, after root exposure to WCS417. The list of proteins identified by
 759 proteomic analysis which are downregulated in the leaves of both wt Col and *atfdh1-5* after two days of root exposure to WCS417 (or to mock
 760 treatment), are reported; the name, AGI code, UniProt ID, annotation, subcellular localization according to Aramemnon ([http://aramemnon.uni-](http://aramemnon.uni-koeln.de)
 761 [koeln.de](http://aramemnon.uni-koeln.de)) and SUBA5 (<https://suba.live/>) (according to their respective highest scores), F ratio and Probability ($P \leq 0.01$) (by LDA), and DAve index
 762 (by MAProMa) are reported. SP: secretory pathway; PM: plasma membrane.

763

Protein name	AGI code	UniProt ID	Annotation	Localization (Aramemnon/SUBA5)	F ratio		Prob > F		DAve	
					wt Col	<i>atfdh1-5</i>	wt Col	<i>atfdh1-5</i>	wt Col	<i>atfdh1-5</i>
CAM7	AT3G43810	A0A1I9LPJ2	Calmodulin 7	SP/cytosol	13	26	5.3E ⁻⁰³	4.8E ⁻⁰⁴	1.03	0.91
CP29B	AT2G37220	Q9ZUU4	RNA-binding protein CP29B	plastid/plastid	14	36	4.1E ⁻⁰³	1.3E ⁻⁰⁴	0.37	0.49
CPN10-2	AT2G44650	O80504	10 kDa chaperonin 2	plastid/plastid	13	19	4.6E ⁻⁰³	1.5E ⁻⁰³	1.49	1.63
CPN20	AT5G20720	O65282	20 kDa chaperonin	plastid/plastid	12	61	5.4E ⁻⁰³	1.5E ⁻⁰⁵	0.36	0.76
CSP2	AT4G38680	Q41188	Cold shock protein 2	nucleus/nucleus	12	13	6.0E ⁻⁰³	4.7E ⁻⁰³	0.73	0.63
ERD10	AT1G20450	P42759	Early responsive to dehydration protein 10	nucleus/cytosol or PM	34	55	1.7E ⁻⁰⁴	2.4E ⁻⁰⁵	0.98	0.95
MEE59	AT4G37300	O23157	maternal effect embryo arrest 59	nucleus/nucleus	25	61	5.4E ⁻⁰⁴	1.5E ⁻⁰⁵	1.44	2.0
F13I12.120	AT3G47070	Q9SD66	thylakoid soluble phosphoprotein	SP/plastid	11	25	7.2E ⁻⁰³	5.7E ⁻⁰⁴	0.96	1.42

PSAE1	AT4G28750	Q9S831	PSI subunit E1	plastid/plastid	56	262	2.2E-05	1.7E-08	0.62	0.70
PSAE2	AT2G20260	Q9S714	PSI subunit E2	plastid/plastid	14	68	3.7E-03	9.1E-06	0.60	0.78
PSB27-1	AT1G03600	Q9LR64	PSII repair protein PSB27-H1	plastid/plastid	32	32	2.1E-04	2.2E-04	0.63	0.94
PSBO2	AT3G50820	Q9S841	Oxygen-evolving enhancer protein 1-2	plastid/plastid	12	155	5.4E-03	2.0E-07	0.31	0.46
PSBP1	AT1G06680	Q42029	Oxygen-evolving enhancer protein 2-1	plastid/plastid	32	28	2.0E-04	3.3E-04	0.55	0.78
RGGA	AT4G16830	O23523	RGG repeats nuclear RNA binding protein A	nucleus/nucleus	12	94	6.7E-03	2.2E-06	1.11	1.89
RGGC	AT5G47210	Q9LVT8	putative RGG repeats nuclear RNA binding protein C	plastid/cytosol	10	30	9.7E-03	2.7E-04	0.92	1.61
RRF	AT3G63190	Q9M1X0	Ribosome-recycling factor	plastid/plastid	14	53	3.6E-03	2.7E-05	1.23	1.22
At2g21530	AT2G21530	Q8GWP4	unknown protein	plastid/plastid	33	13	1.8E-04	4.8E-03	1.44	2.0
At5g02570	AT5G02570	Q9LZ45	Histone H2B.9	nucleus/nucleus	16	22	2.4E-03	8.9E-04	2.0	1.29
At5g24165	AT5G24165	Q8LDQ8	unknown protein	plastid/mitoch	12	14	6.7E-03	4.0E-03	1.17	1.15

764

765

766

767 **Table 3**

768 Proteins with antioxidant function, which are differentially expressed in wt Col and/or *atfdh1-5* leaves after two days root exposure to WCS417. For
 769 each of them, the name, AGI code, annotation, subcellular localization according to Aramemnon (<http://aramemnon.uni-koeln.de>) and to SUBA5
 770 (<https://suba.live/>) according to their respective highest scores, and the average Peptide Spectrum Matches (PSMs) per condition are reported. For
 771 each enzyme, statistically significant differences between mock and WCS417-treated values, within same genotype, are indicated with *; “/” indicates
 772 that the given protein has not been detected, in the proteome analysis, under that experimental condition. SP: secretory pathway.

773
 774

Protein name	AGI code	UniProt ID	Annotation	Localization (Aramemnon/ SUBA5)	Av PSMs mock		Av PSMs WCS417	
					wt Col	<i>atfdh1-5</i>	wt Col	<i>atfdh1-5</i>
APX1	AT1G07890	Q05431	L-ascorbate peroxidase 1	mitoch/	3.7	8.5	6.2	12.5*
GSTF2	AT4G02520	P46422	Glutathione S-transferase F2	mitoch/	7.3	21.5	22.4*	19.5
GSTF7	AT1G02920	Q9SRY5	Glutathione S-transferase F7	mitoch/cytosol	/	/	1.8*	2.8*
GSTF8	AT2G47730	Q96266	Glutathione S-transferase F8	plastid/plastid	2.0	2.6	5.7*	8.9*
GSTF9	AT2G30860	O80852	Glutathione S-transferase F9	mitoch/	2.5	9.6	7.6*	7.9
GSTF10	AT2G30870	P42761	Glutathione S-transferase F10	mitoch/	0.9	2.2	2.6	5.1*
GSTU19	AT1G78380	Q9ZRW8	Glutathione S-transferase U19	SP/	0.3	0.2	0.4	4.5*

791
 792

793 **Figure legends**

794 **Figure 1**

795 GUS staining of *A. thaliana Vu* FDH::GUS seedlings after *in vitro* co-cultivation with WCS417. **(A)**
 796 Seven days old *Vu* FDH::GUS seedlings were cultivated *in vitro* for 2 or 7 days on MS agar plates
 797 with WCS417 or MgSO₄ (mock condition), avoiding contact with the root apparatus. A schematic
 798 representation of the experiment is shown. **(B)** GUS staining of 7 days WCS417-treated or **(C)** mock-
 799 treated seedlings: details of leaves and root apparatus are shown, and the hydathodes are indicated by
 800 red arrows. Scale bars represent 1 mm. **(D)** Number of stained hydathodes after 2 or 7 days of
 801 exposure to WCS417, with respect to the mock treatment, as described in **(B)** and **(C)**; each bar
 802 represents the mean value \pm SE of stained hydathodes measured in at least 24 seedlings collected
 803 from 3 different plates (at least 8 seedlings per plate). Significant differences in WCS417-treated with
 804 respect to mock-treated, according to the t-test, are indicated by * ($P < 0.05$) or ** ($P < 0.01$). Panel
 805 1A was created using BioRender.com

806

807 **Figure 2**

808 GUS-staining of hydathodes in *A. thaliana Vu* FDH::GUS leaves after *in vivo* root exposure to
 809 WCS417. **(A)** Leaves from 4 weeks old plants grown in soil were stained for GUS activity before
 810 inoculation (control), and after 2 days of WCS417 or MgSO₄ (mock) inoculation in the soil (indicated
 811 as WCS417 or mock, respectively); each bar represents the mean value \pm SE of stained hydathodes
 812 in 12 (control) or 36 (WCS417, mock) GUS-stained leaves. Significant differences between
 813 WCS417-and mock-treated values, according to the t-test, are indicated with ** ($P < 0.01$). **(B)**
 814 Leaves from 4 weeks old plants grown in soil were stained for GUS activity before inoculation
 815 (control) and after 4 days from the WCS417 or MgSO₄ (mock) inoculation in the soil (indicated as
 816 WCS417 or mock, respectively); leaves sampled from plants close (but without any contact) to either
 817 the WCS417- or mock-treated ones ('close to WCS417' and 'close to mock', respectively) were also
 818 GUS-stained. Bars represent the mean number \pm SE of stained hydathodes in 73 (control), 82 (mock),

819 100 (WCS417), 90 (close to mock), and 99 (close to WCS417) GUS-stained leaves. Significant
 820 differences between WCS417- and mock-treated values are indicated by ** ($P \leq 0.01$) according to
 821 the t-test.

822

823 **Figure 3**

824 WCS417 colonization of *A. thaliana* wt Col and *atfdh1-5* roots. wt and *atfdh1-5* seedlings were grown
 825 for 13 days in ½ MS plates (around 30 seedlings of each line/plate). For each plate, 100 µl of WCS417
 826 suspension (10^7 CFU ml⁻¹) were evenly distributed at the bottom of the hypocotyls of each line and
 827 the CFU gr⁻¹ roots was evaluated after 2 days from the infection. Each bar represents the mean value
 828 ± SE (in log) from three independent plates. Significant difference is indicated by * ($P < 0.05$)
 829 according to the t-test.

830

831 **Figure 4**

832 Proteomic analysis of *A. thaliana* wt Col and *atfdh1-5* leaves after root exposure to WCS417. Roots
 833 of 4 weeks old *A. thaliana* wt Col and *atfdh1-5* plants were exposed for 2 days to WCS417 (or mock),
 834 and total proteins were then extracted for proteomic analysis. For each line and treatment, 3 biological
 835 x 2 technical replicates were analyzed (n = 6). (A) 2D Map showing the distribution of identified
 836 proteins by pI, MW, and global average Peptide Spectrum Matches (PSMs). (B) Venn diagrams of
 837 the number of identified proteins in pairwise comparison: wt Col mock vs wt Col WCS417; *atfdh1-5*
 838 mock vs *atfdh1-5* WCS417; wt Col mock vs *atfdh1-5* mock; wt Col WCS417 vs *atfdh1-5* WCS417.

839

840 **Figure 5**

841 Proteomic analysis of *A. thaliana* wt Col and *atfdh1-5* leaves after root exposure to WCS417.
 842 Hierarchical clustering of proteins differentially expressed (LDA, $P \leq 0.01$) by comparing (A) wt Col
 843 mock vs wt Col WCS417, (B) *atfdh1-5* mock vs *atfdh1-5* WCS417, (C) wt Col mock vs *atfdh1-5*
 844 mock, (D) wt Col WCS417 vs *atfdh1-5* WCS417. (E) Spearman's correlation values r by comparing,

845 in pairs, proteins identified as differentially expressed (LDA, $P \leq 0.05$). For each graph, the
846 coordinates indicate the spectral counts of a protein in the two analyzed conditions.

847

848

849 **Supplementary Material descriptions**

850 **Figure S1.** The *A. thaliana atfdh1-5* mutant is more susceptible to the virulent
851 *Xanthomonas campestris* pv. *campestris* strain 8004DxopAC.

852 **Figure S2.** Photochemical parameters of *A. thaliana* wt Col leaves after WCS417
853 treatment.

854 **Figure S3** *A. thaliana* plants grown in soil to test the involvement of volatile
855 compounds in WCS417-induced FDH expression.

856 **Figure S4** *A. thaliana* wt Col and *atfdh1-5* mutant after exposure to WCS417.

857 **Figure S5.** Details of wt Col roots from seedlings grown for 7 days in MS plates and
858 then exposed for 7 more days to mock treatment.

859 **Figure S6** Details of wt Col roots from seedlings grown for 7 days in MS plates and
860 then exposed for 7 more days to WCS417.

861 **Figure S7** Details of *atfdh1-5* roots from seedlings grown for 7 days in MS plates and
862 then exposed for 7 more days to mock treatment.

863 **Figure S8** Details of *atfdh1-5* roots from seedlings grown for 7 days in MS plates and
864 then exposed for 7 more days to WCS417.

865 **Figure S9.** Five weeks old *A. thaliana* wt Col and *atfdh1-5* mutant at d0, i.e. before
866 treatment with WCS417 (or mock).

867 **Figure S10** Fresh weight and chlorophyll content of *A.thaliana* wt Col and *atfdh1-5*
868 plants, after WCS417 treatment.

869 **Figure S11** *A. thaliana* wt Col and *atfdh1-5* rosette leaves after exposure to WCS417
870 for proteomic analysis.

871 **Figure S12** Staining of *A. thaliana* wt Col and *atfdh1-5* rosette leaves with
872 diaminobenzidine (DAB) after exposure to WCS417 for proteomic analysis.

873 **Table S1** Proteins identified by LC-MS/MS from *A. thaliana* leaves wt Col mock,
874 *atfdh1-5* mock, wt Col WCS417-treated, *atfdh1-5* WCS417-treated.

875 **Table S2** Differentially expressed proteins (DEPs) by comparing the protein profiles
876 from *A. thaliana* leaves of wt Col mock, *atfdh1-5* mock, wt Col WCS417-treated,
877 *atfdh1-5* WCS417-treated.

878 **Table S3** *A.thaliana* wt Col proteins with altered expression, in 4 weeks old leaves
879 after roots exposure for two days to WCS417, when compared to expression after mock
880 treatment.

881 **Table S4** *A. thaliana atfdh1-5* proteins with altered expression, in 4 weeks old leaves
882 after roots exposure for two days to WCS417, when compared to expression after mock
883 treatment.

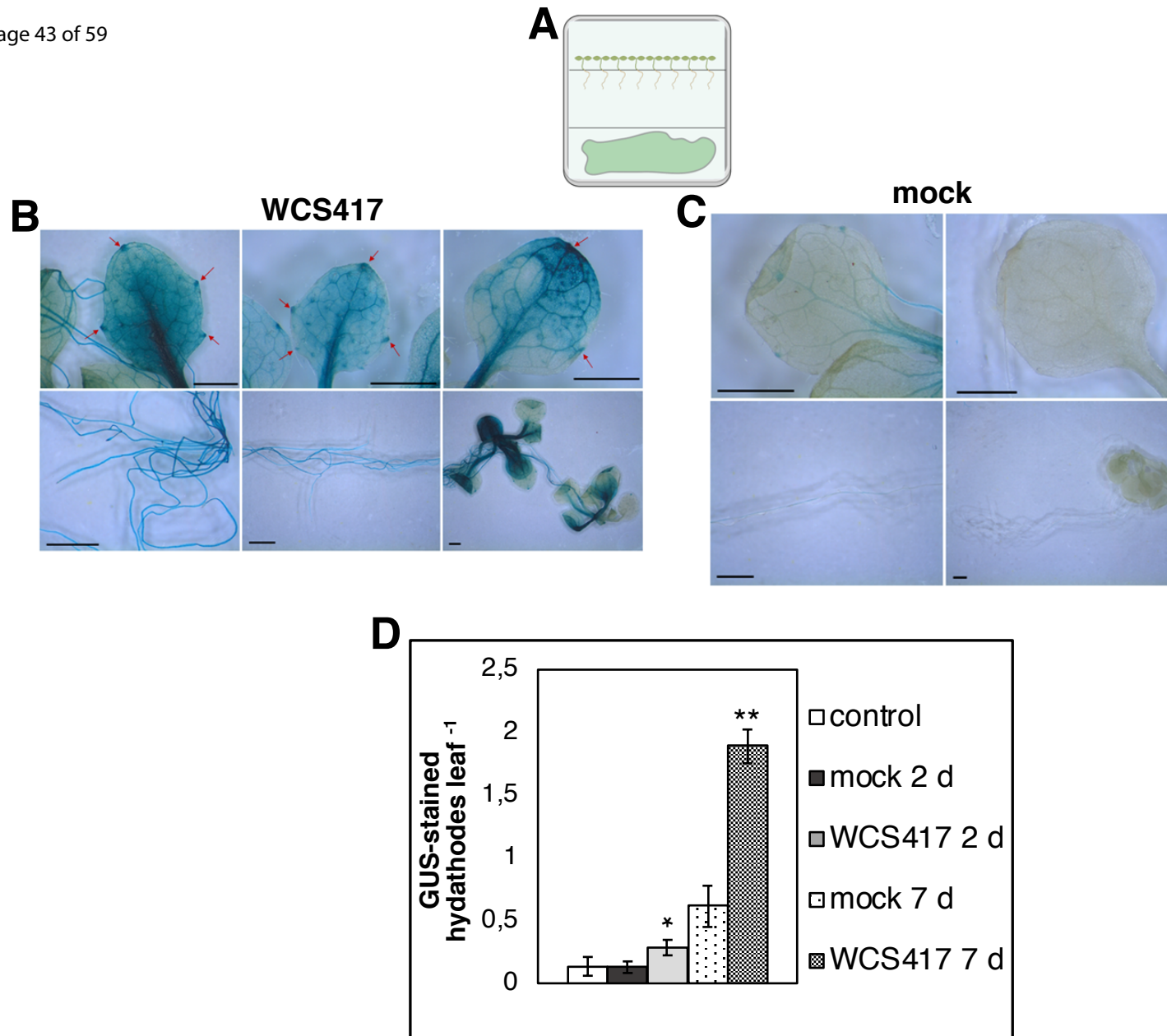
884 **Table S5** KEGG pathways differentially enriched by comparing the protein profiles
885 from *A. thaliana* leaves wt Col mock, *atfdh1-5* mock, wt Col WCS417-treated, *atfdh1-*
886 *5* WCS417-treated.

887 **Table S6** (A) List of DEPs ($P \leq 0.01$) proteins, by comparing *A. thaliana* wt Col and
888 *atfdh1-5* in mock condition. (B) List of DEPs ($P \leq 0.01$) proteins, by comparing *A.*
889 *thaliana* wt Col and *atfdh1-5* after exposure to WCS417.

890

891

892

**Figure 1**

GUS staining of *A. thaliana* *Vu* FDH::GUS seedlings after *in vitro* co-cultivation with WCS417. **(A)** Seven days old *Vu* FDH::GUS seedlings were cultivated *in vitro* for 2 or 7 days on MS agar plates with WCS417 or MgSO₄ (mock condition), avoiding contact with the root apparatus. A schematic representation of the experiment is shown. **(B)** GUS staining of 7 days WCS417-treated or **(C)** mock-treated seedlings: details of leaves and root apparatus are shown, and the hydathodes are indicated by red arrows. Scale bars represent 1 mm. **(D)** Number of stained hydathodes after 2 or 7 days of exposure to WCS417, with respect to the mock treatment, as described in **(B)** and **(C)**; each bar represents the mean value \pm SE of stained hydathodes measured in at least 24 seedlings collected from 3 different plates (at least 8 seedlings per plate). Significant differences in WCS417-treated with respect to mock-treated, according to the t-test, are indicated by * ($P < 0.05$) or ** ($P < 0.01$). Panel 1A was created using BioRender.com

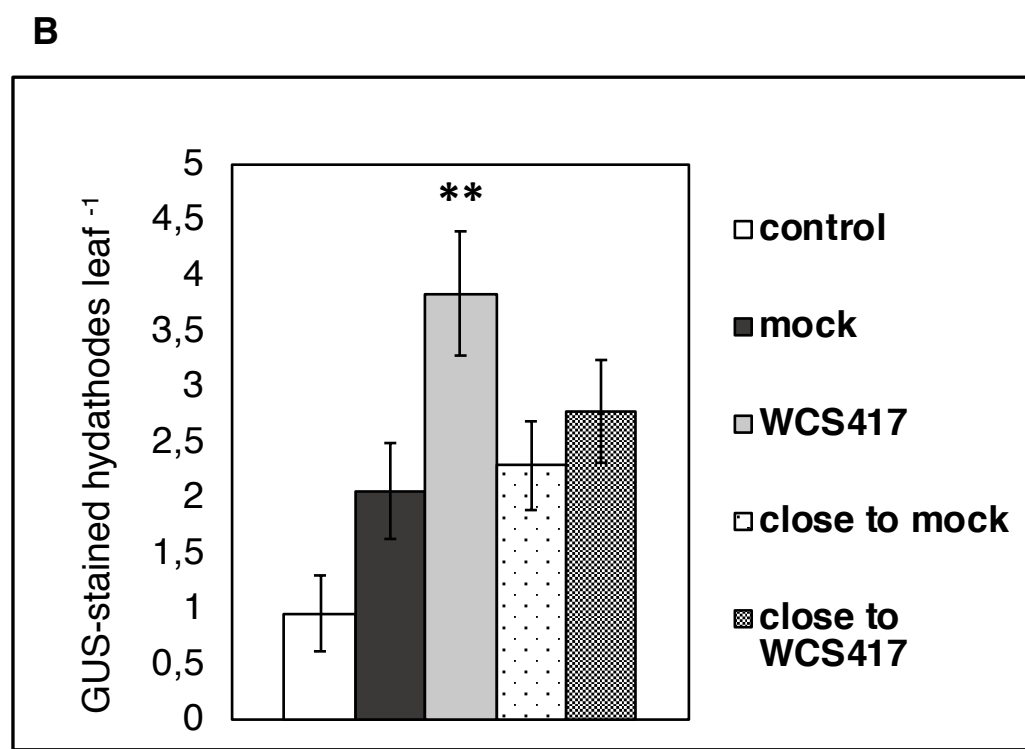
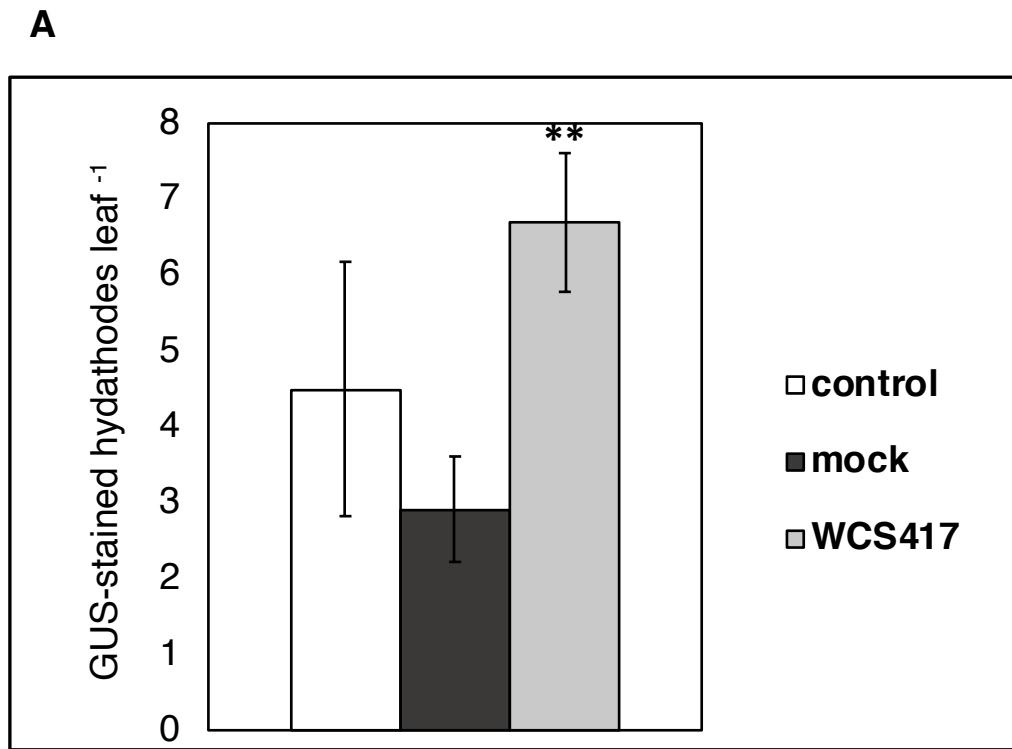


Figure 2 GUS-staining of hydathodes in *A. thaliana* *Vu* FDH::GUS leaves after *in vivo* root exposure to WCS417. **(A)** Leaves from 4 weeks old plants grown in soil were stained for GUS activity before inoculation (control), and after 2 days of WCS417 or MgSO₄ (mock) inoculation in the soil (indicated as WCS417 or mock, respectively); each bar represents the mean value \pm SE of stained hydathodes in 12 (control) or 36 (WCS417, mock) GUS-stained leaves. Significant differences between WCS417- and mock-treated values, according to the t-test, are indicated with ** ($P < 0.01$). **(B)** Leaves from 4 weeks old plants grown in soil were stained for GUS activity before inoculation (control) and after 4 days from the WCS417 or MgSO₄ (mock) inoculation in the soil (indicated as WCS417 or mock, respectively); leaves sampled from plants close (but without any contact) to either the WCS417- or mock-treated ones ('close to WCS417' and 'close to mock', respectively) were also GUS-stained. Bars represent the mean number \pm SE of stained hydathodes in 73 (control), 82 (mock), 100 (WCS417), 90 (close to mock), and 99 (close to WCS417) GUS-stained leaves. Significant differences between WCS417- and mock-treated values are indicated by ** ($P \leq 0.01$) according to the t-test.

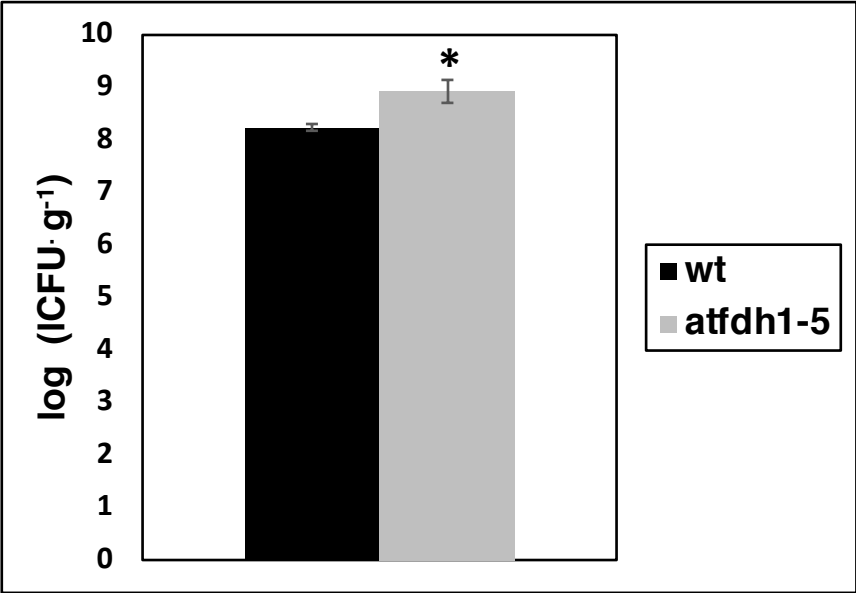
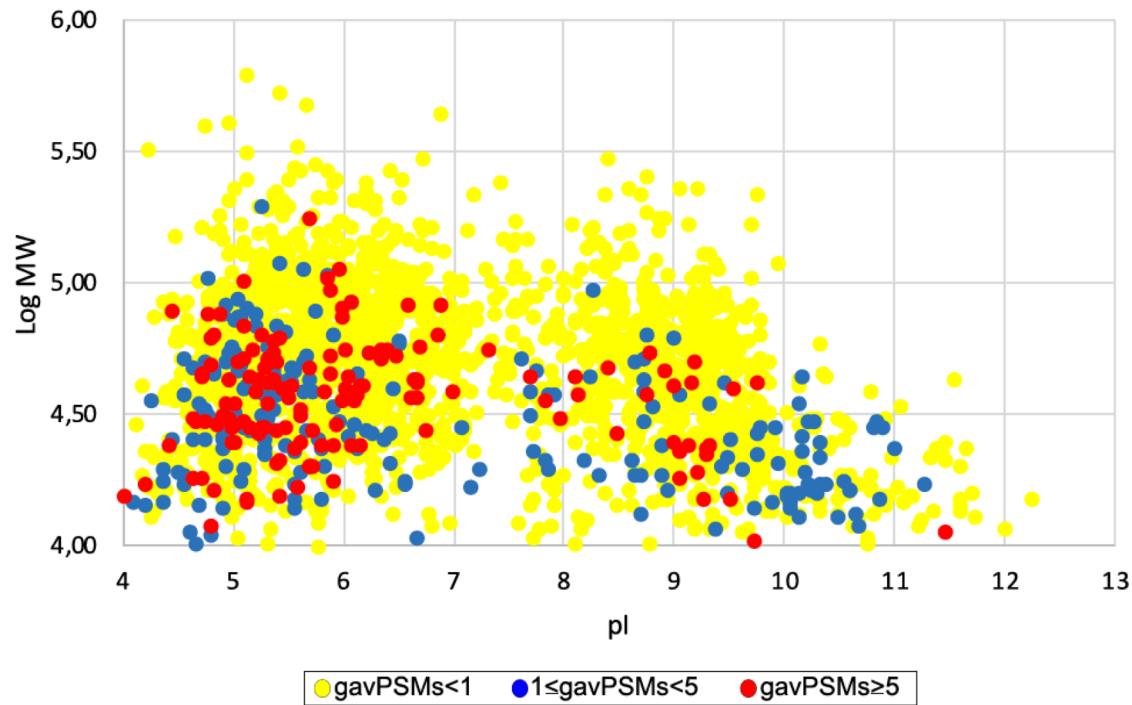


Figure 3 WCS417 colonization of *A. thaliana* wt Col and *atfdh1-5* roots. wt and *atfdh1-5* seedlings were grown for 13 days in ½ MS plates (around 30 seedlings of each line/plate). For each plate, 100 µl of WCS417 suspension (10⁷ CFU ml⁻¹) were evenly distributed at the bottom of the hypocotyls of each line and the CFU gr⁻¹ roots was evaluated after 2 days from the infection. Each bar represents the mean value ± SE (in log) from three independent plates. Significant difference is indicated by * (*P* < 0.05) according to the t-test.

A



B

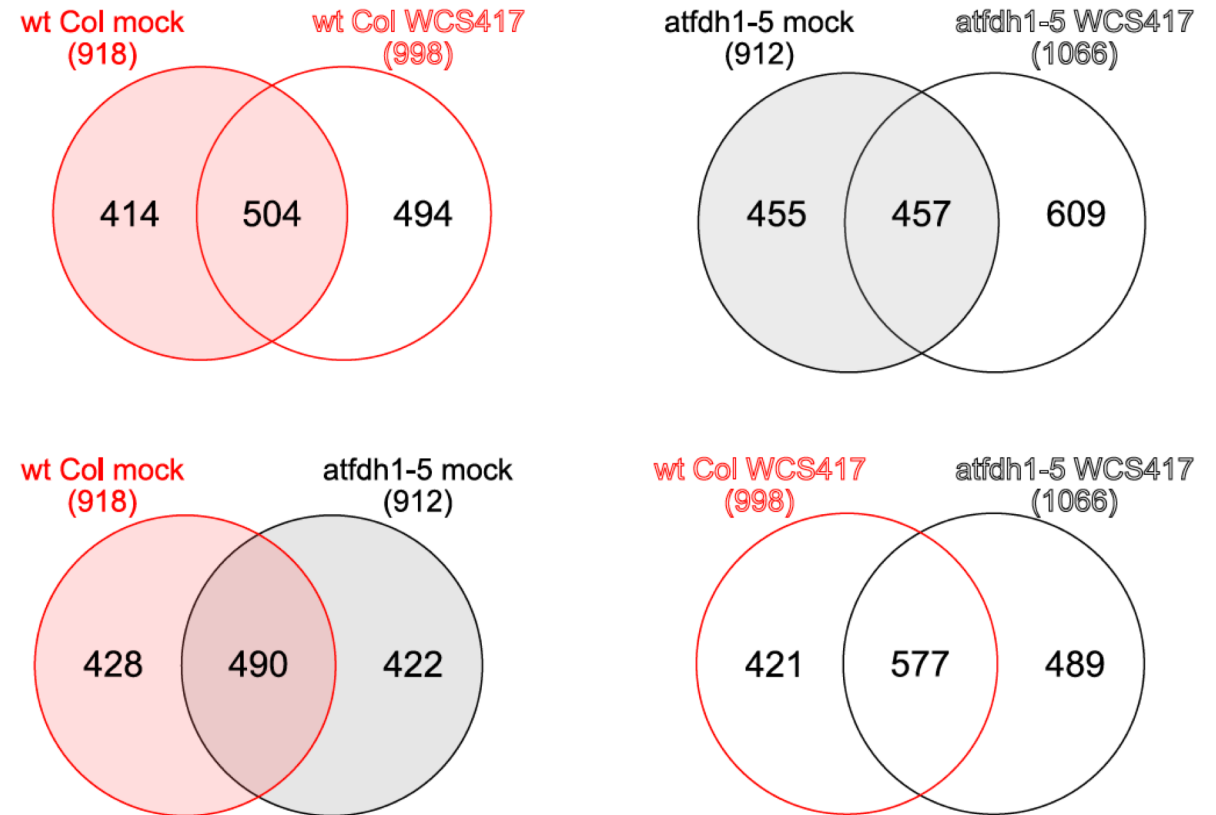
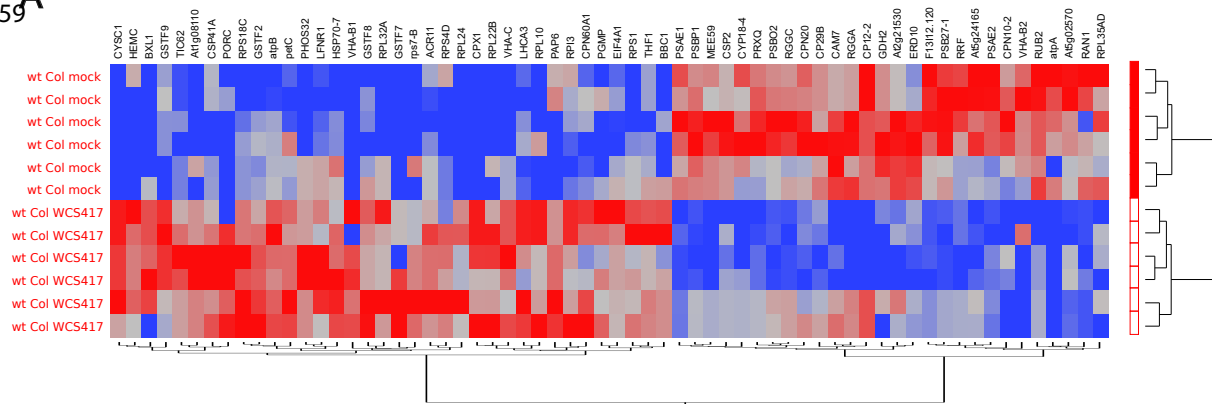
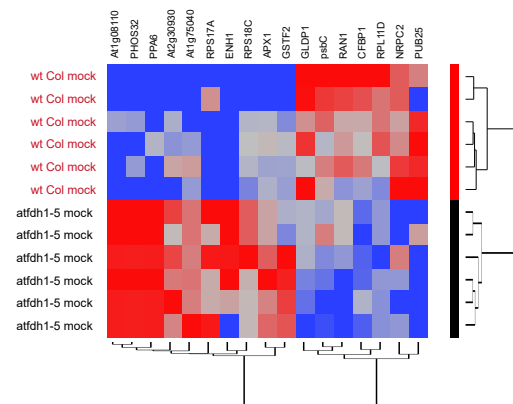


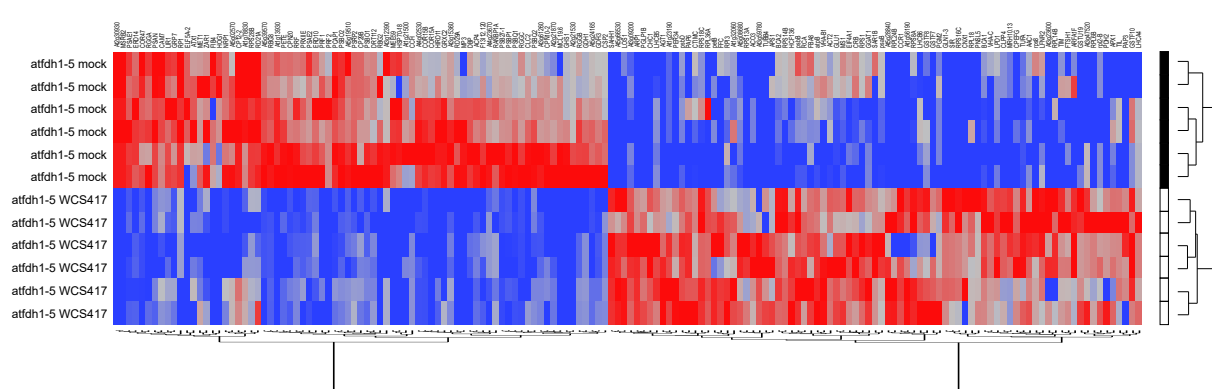
Figure 4 Proteomic analysis of *A. thaliana* wt Col and *atfdh1-5* leaves after root exposure to WCS417. Roots of 4 weeks old *A. thaliana* wt Col and *atfdh1-5* plants were exposed for 2 days to WCS417 (or mock), and total proteins were then extracted for proteomic analysis. For each line and treatment 3 biological x 2 technical replicates were analyzed (n = 6). **(A)** 2D Map showing the distribution of identified proteins by pI, MW, and global average Peptide Spectrum Matches (PSMs). **(B)** Venn diagrams of the number of identified proteins in pairwise comparison: wt Col mock vs wt Col WCS417; *atfdh1-5* mock vs *atfdh1-5* WCS417; wt Col mock vs *atfdh1-5* mock; wt Col WCS417 vs *atfdh1-5* WCS417.



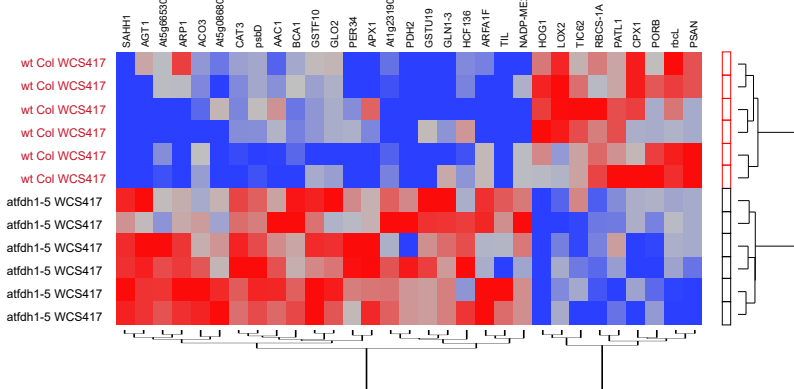
C



B



D



E

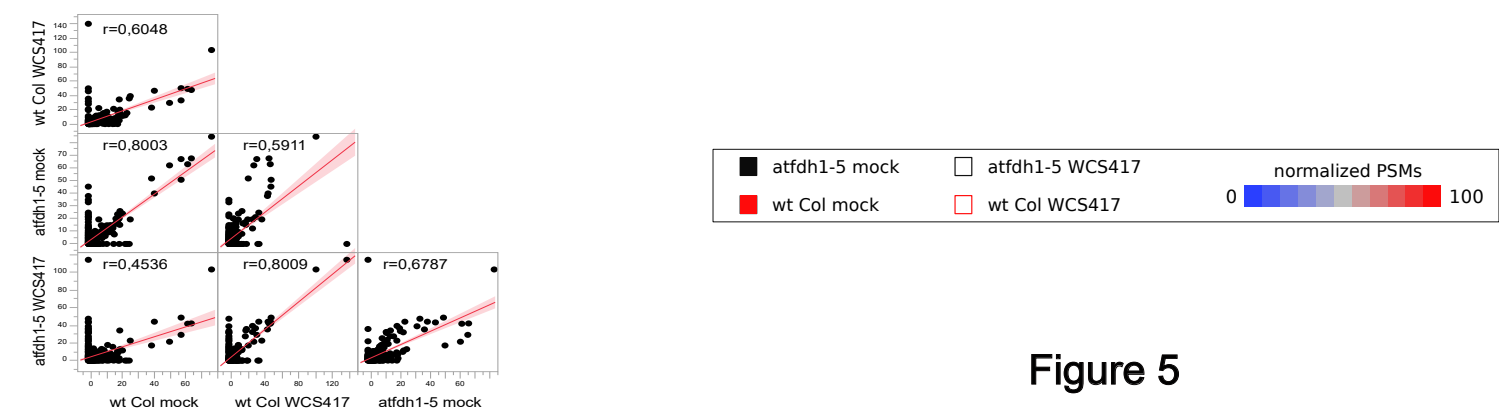


Figure 5

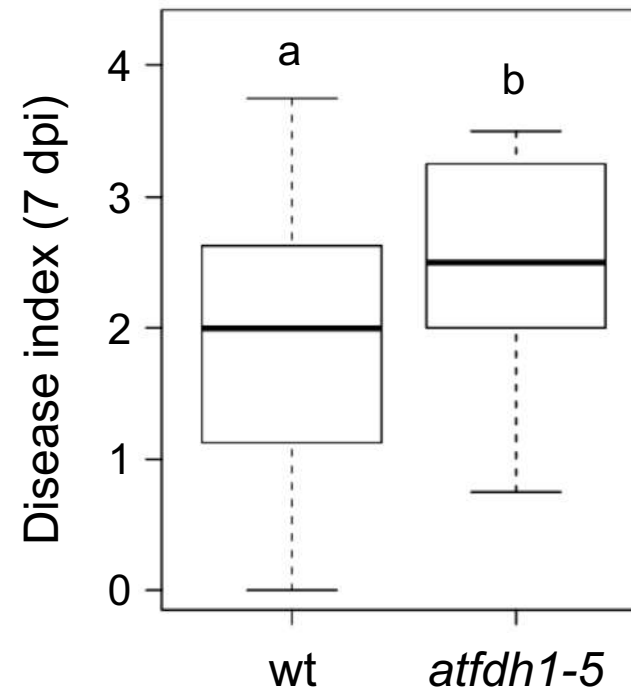


Figure S1. The *A. thaliana atfdh1-5* mutant is more susceptible to the virulent *Xanthomonas campestris* pv. *campestris* strain 8004 Δ *xopAC*. The disease index (DI) was scored 7 days after wound-inoculation of *A. thaliana* wt Col or *atfdh1-5* mutant with bacterial suspensions at 10^8 CFU \cdot mL $^{-1}$. Five independent experiments were performed (four plants, four leaves per plate) and combined using the median DI for each plant. Statistically significant differences were determined using HSD test (p -value $<$ 0.05) and are indicated by different letters.

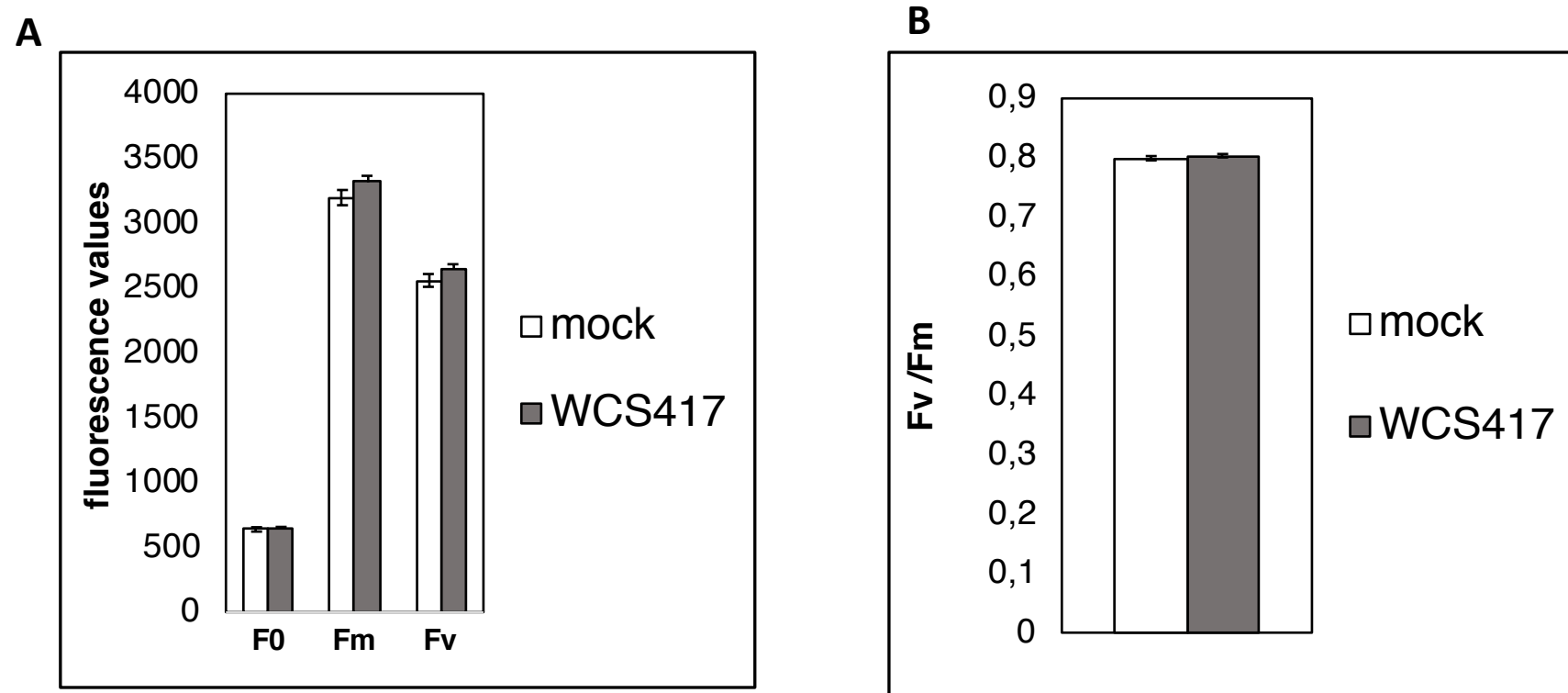


Figure S2. Photochemical parameters of *A. thaliana* wt Col leaves after WCS417 treatment. Roots of 4 weeks old *A. thaliana* wt Col plants grown in soil plant were exposed to WCS417 or MgSO₄ (mock), and their leaves were sampled after 2 days to evaluate (A) F₀ (initial fluorescence), F_m (maximum fluorescence), F_v (variable fluorescence), and (B) F_v/F_m (maximal photochemical efficiency). Each bar represents the mean value ± SE from at least 20 independent leaves.

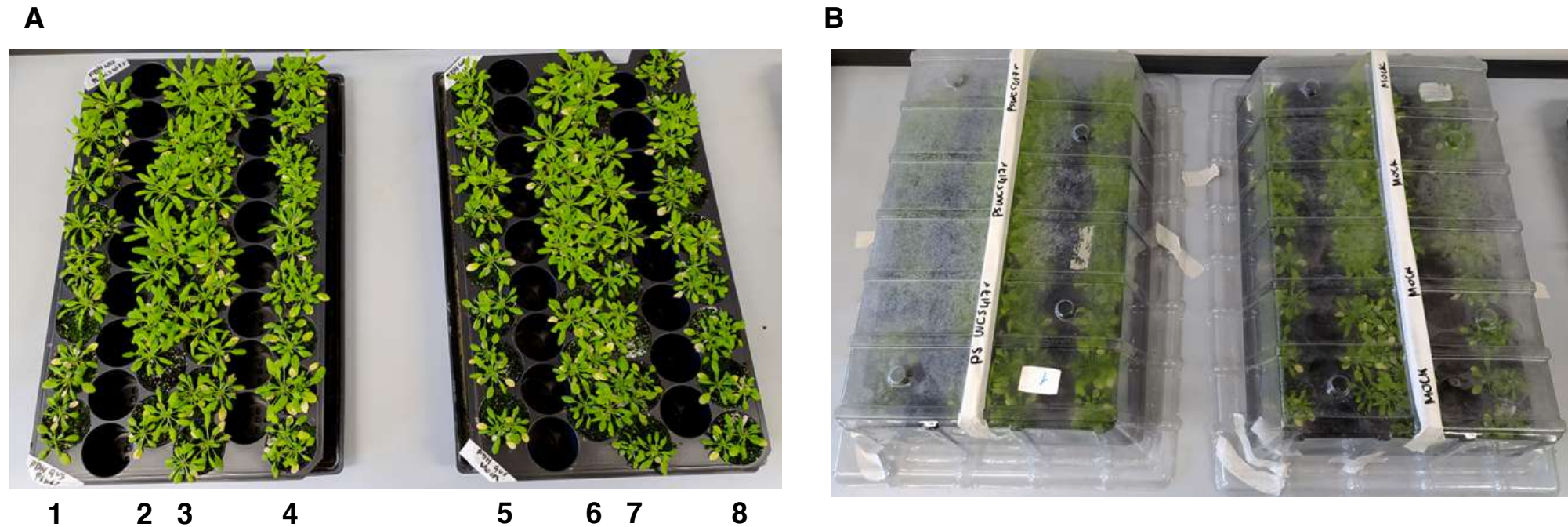
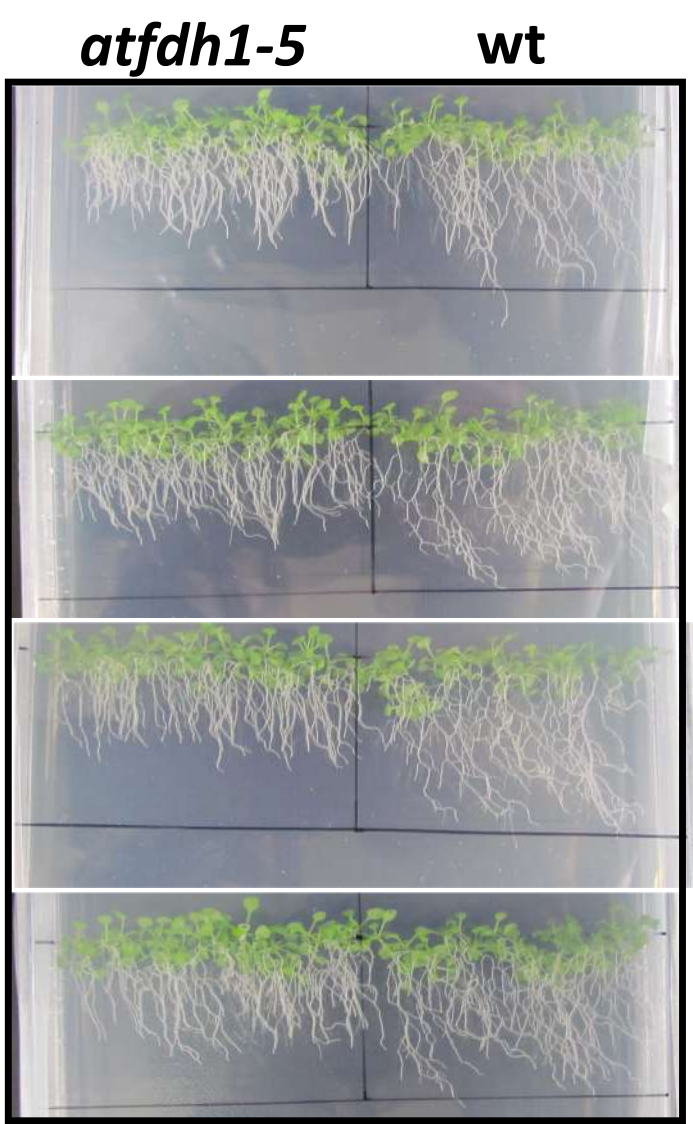


Figure S3 *A. thaliana* plants grown in soil to test the involvement of volatile compounds in WCS417-induced FDH expression. **(A)** 4 weeks old *A. thaliana* *Vu* FDH::GUS plants grown in soil: only those in the central rows were inoculated with either WCS417 (rows 2, 3) or MgSO_4 (mock, rows 6, 7). The two external rows of plants (lines 1, 4, 5, 8) did not receive any inoculum. **(B)** The Aratrays containing the treated plants were covered, after treatment, with transparent lids without holes.



7 d mock



7 d WCS417

Figure S4

A. thaliana wt Col and *atfdh1-5* mutant after exposure to WCS417. *wt* and *atfdh1-5* lines germinated on MS plates have been exposed, after 7 days, to WCS417 (or mock treatment) for 7 more days, without any initial contact between WCS417 and seedlings. Pictures of four different plates per treatment, each containing both lines, are shown.



Figure S5. Details of *wt Col* roots from seedlings grown for 7 days in MS plates and then exposed for 7 more days to mock treatment. Bar corresponds to 1 mm.

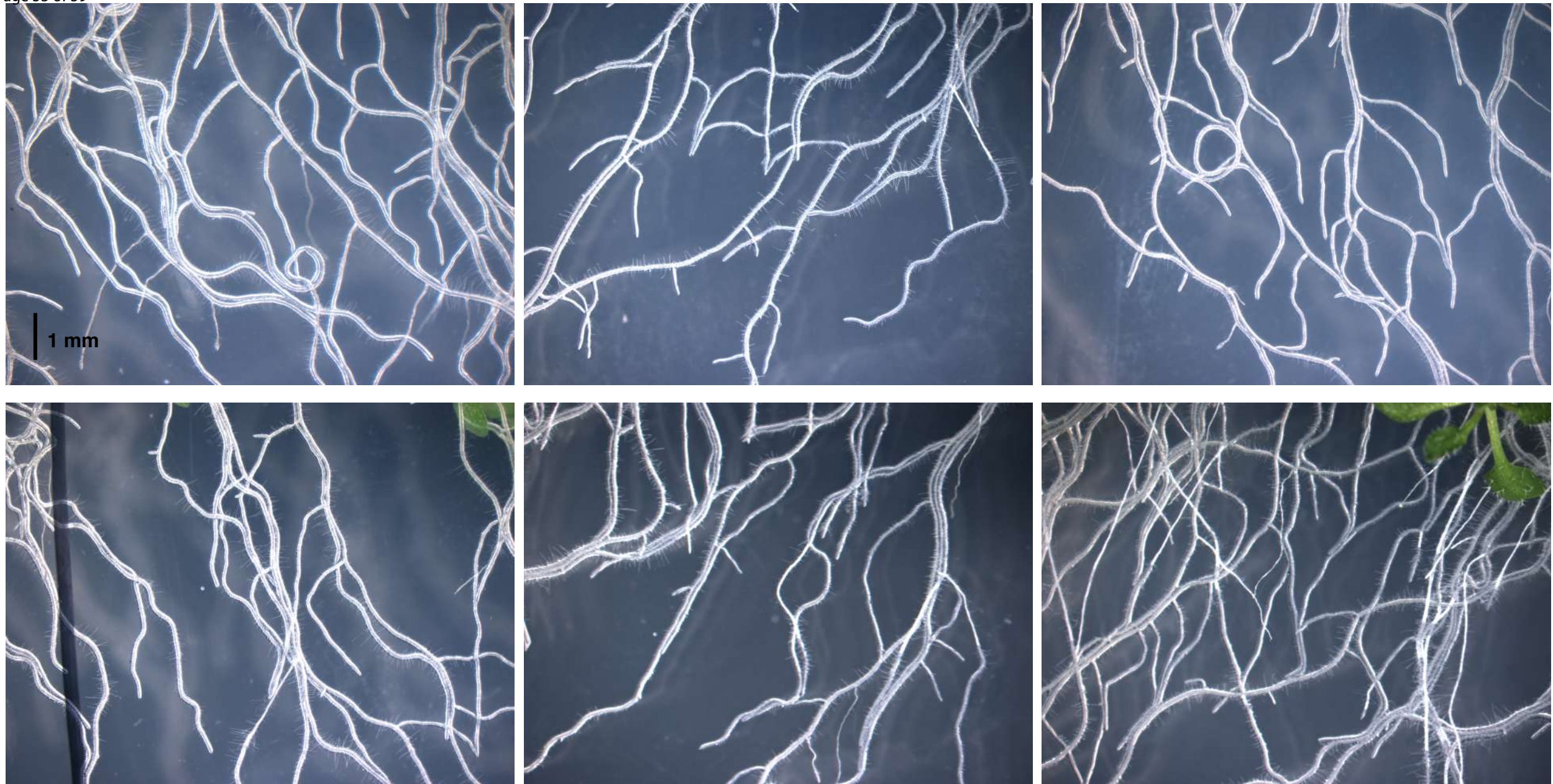


Figure S6 Details of wt Col roots from seedlings grown for 7 days in MS plates and then exposed for 7 more days to WCS417. Bar corresponds to 1 mm.



Figure S7 Details of *atfdh1-5* roots from seedlings grown for 7 days in MS plates and then exposed for 7 more days to mock treatment. Bar corresponds to 1 mm.



Figure S8 Details of *atfdh1-5* roots from seedlings grown for 7 days in MS plates and then exposed for 7 more days to WCS417. Bar corresponds to 1 mm.

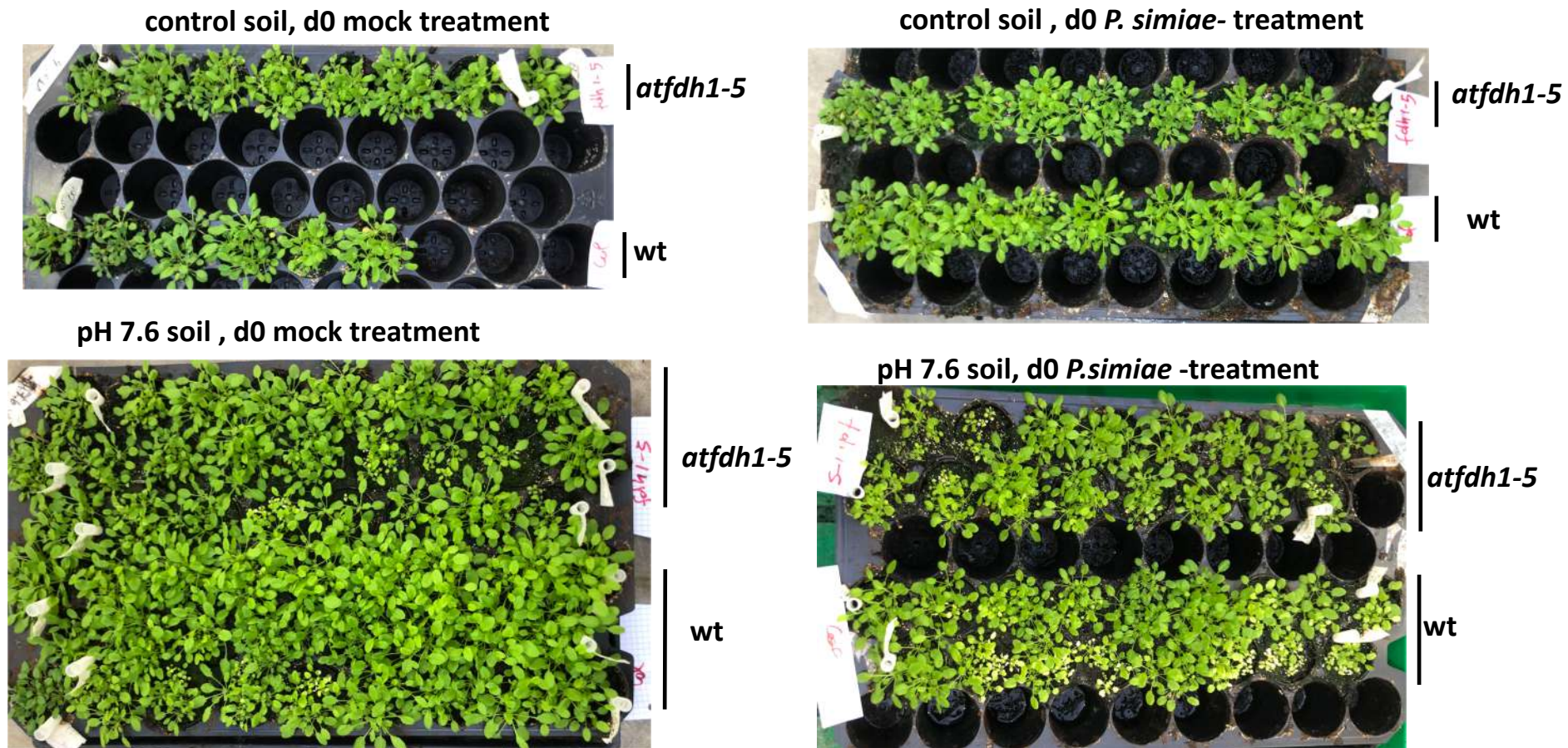


Figure S9. Five weeks old *A. thaliana* wt Col and *atfdh1-5* mutant at d0, i.e. before treatment with WCS417 (or mock). Both lines were grown on either control or alkaline soil (pH 7.6).

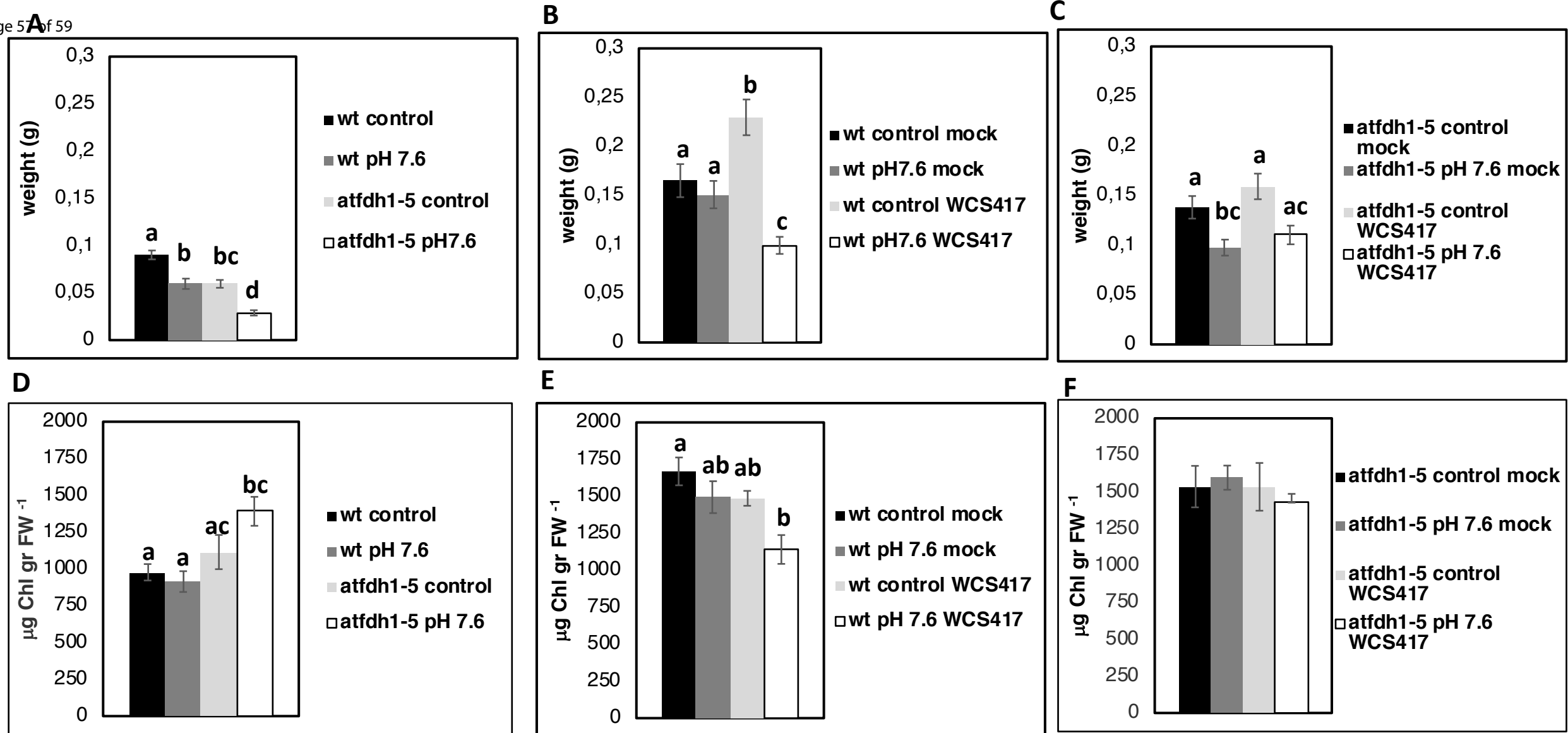


Figure S10 Fresh weight and chlorophyll content of *A.thaliana* wt Col and *atfdh1-5* plants, after WCS417 treatment. Roots of 5 weeks old wt Col and *atfdh1-5* plants, grown on either control or alkaline (pH 7.6) soil, were exposed to WCS417 (or mock treatment, MgSO₄) and rosettes were sampled after 8 days, for measurements. (A) Fresh weight and (D) chlorophyll content ($\mu\text{g chlorophyll gr FW}^{-1}$) of single rosettes before soil treatment with WCS417 (d0). Fresh weight of single rosettes of (B) wt Col and (C) *atfdh1-5*, and chlorophyll content of (E) wt Col and (F) *atfdh1-5*, after 8 days from treatment (d8). Bars in (A,B,C) are mean values \pm SE of at least 32 rosettes, bars in (D,E,F) are mean values \pm SE of 5 independent samples, each containing at least 10 leaves. Different letters indicate significant differences, according to ANOVA and Tukey's test ($p < 0.05$).

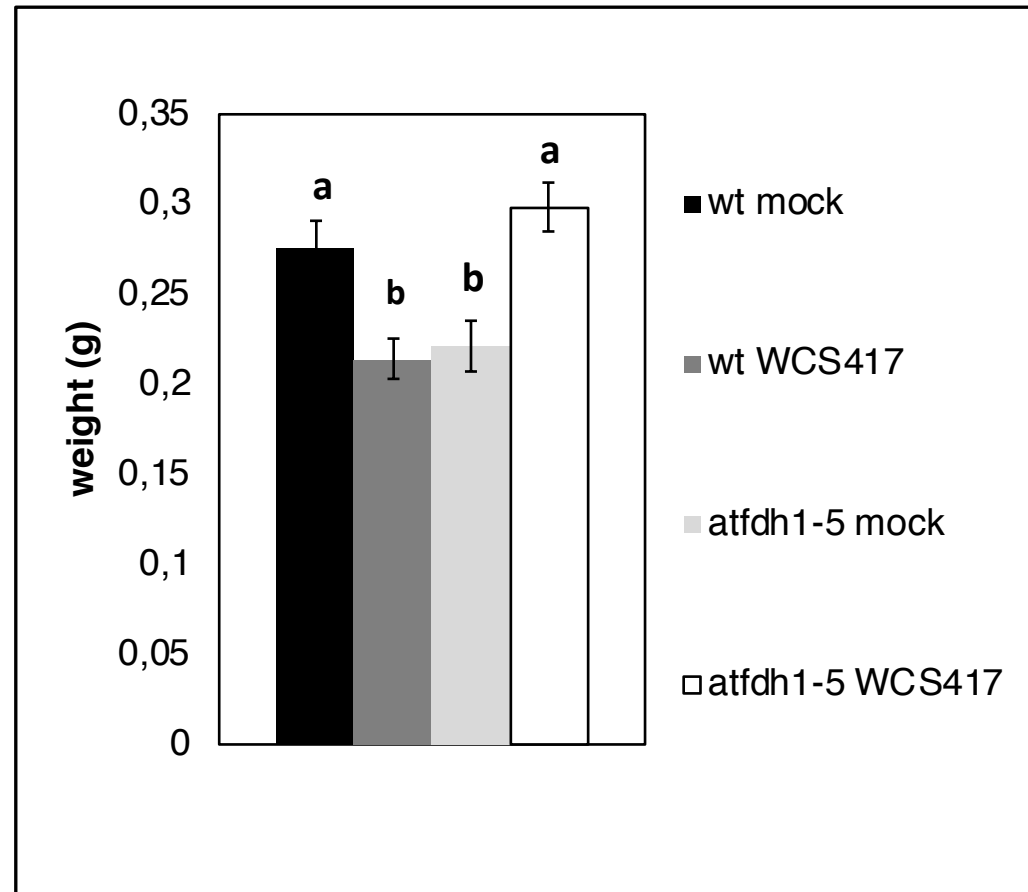


Figure S11 *A. thaliana* wt Col and *atfdh1-5* rosette leaves after exposure to WCS417 for proteomic analysis. Rosettes of *A. thaliana* wt Col and mutant *atfdh1-5* plants were sampled after two days of root exposure to WCS417 for proteomic analysis. Each bar represents the mean fresh weight of a single rosette (g) \pm SE, from 20 rosettes. Significant differences between WCS417-treated and mock-treated samples, according to ANOVA, followed by Tukey's test, are indicated with different letters ($P < 0.05$).



Figure S12 Staining of *A. thaliana* wt Col and *atfdh1-5* rosette leaves with diaminobenzidine (DAB) after exposure to WCS417 for proteomic analysis. Rosette leaves of *A. thaliana* wt Col and *atfdh1-5* plants sampled after 2 days of root exposure to WCS417 were stained with DAB for H_2O_2 detection. Bars represent 1 cm.